EXPERIMENTAL EXAMINATION OF NOZZLE GEOMETRY ON WATER JET IN A SUBSONIC CROSSFLOW

BY

BAAFOUR NYANTEKYI-KWAKYE

A Thesis
Submitted to the Faculty of Graduate Studies of
The University of Manitoba
In Partial Fulfillment of the Requirements for the Degree of

MASTER OF SCIENCE

Department of Mechanical and Manufacturing Engineering
University of Manitoba
Winnipeg, Manitoba
Canada

THE UNIVERSITY OF MANITOBA

FACULTY OF GRADUATE STUDIES

****

COPYRIGHT PERMISSION PAGE

Experimental Examination of Nozzle Geometry on Water Jet in a Subsonic Crossflow

By

BAAFOUR NYANTEKYI-KWAKYE

A Thesis/Practicum submitted to the faculty of graduate studies of the University of Manitoba in partial fulfillment of the Requirements for the Degree

of

Master of Science

ABSTRACT

The effect of a nozzle's internal geometry was studied experimentally to determine the breakup of the emitted water jet when it was injected perpendicularly into a quiescent atmosphere or a subsonic air crossflow. The nozzle's diameter, nominal surface roughness, length-to-diameter ratio and contraction angle were varied, together with the injection pressure, to find the water column's breakup length. Photographs of the water jet at the nozzle's exit, gave a clue as to identify the occurrence of cavitation and a hydraulic flip. On the other hand the water column's breakup length and trajectory, in a subsonic crossflow, were measured by using a stroboscope in conjunction with a high speed CCD camera. Results agreed with previous literature that the breakup length grew with greater liquid/air momentum flux ratios for non-cavitating flows. This was true regardless of the injector nozzle. The rate of increase decreased at the inception of cavitation. On the other hand even shorter breakup lengths were observed at the inception of a hydraulic flip due to the detachment of the water jet from the internal surface of the nozzle. Increasing the nozzle's length-to-diameter ratio eliminated the occurrence of hydraulic flip. The jet's trajectory was correlated with the liquid/air momentum flux ratio and the nozzle's exit diameter. The results showed that higher water jet trajectories were measured under non-cavitating conditions. Even shorter jet trajectories were measured at the inception of a hydraulic flip.

ACKNOWLEDGEMENTS

I would first of all give thanks to Jehovah God for granting me this opportunity and for how far He has brought me. The hard work of Prof. Madjid Birouk and Prof. Neil Popplewell in supervising this work is greatly appreciated. I acknowledge their continual guidance, encouragement and constructive criticism to ensure a distinctive quality work. Their support is greatly appreciated.

As draining as research can be, I always drew strength from the unflinching love, care and support of my family. I am grateful to my parents, Mr. and Mrs. Kofi Nyantekyi-Kwakye and my siblings Nana Agyei and Akwasi Asubonteng. I appreciate the love, support and guidance of my Young Adult Pastor, Rev. Andrew Bawa; I would not be where I am now without him. I also acknowledge all the Pastors and members of Immanuel Fellowship Church.

The training received from Dr. Christopher O. Iyogun is greatly acknowledged. The contribution of Darryl Keith Stoyko in helping with the MATLAB code for the data analysis is not overlooked. The technical and friendly support of Sean Fabbro and John Finken are appreciated greatly. The support and advice of Kwadwo Owusu Poku and all my friends who helped in the course of this pursuit are greatly acknowledged.

DEDICATION

This thesis is dedicated to the Almighty God for granting me the opportunity to study in this challenging research area

TABLE OF CONTENTS

LIST OF TABLES

LIST OF FIGURES

NOMENCLATURE

d nozzle diameter

q Liquid/air momentum flux ratio, $\rho_j v_j^2 / \rho_\infty u_\infty^2$

u crossflow flow axial velocity components in the x direction

v_j water jet's speed at the nozzle exit

V volume of discharged water

$\dot{Q}$ volumetric flow rate

t time elapsed for water collection

A cross-sectional area of the nozzle

x distance in the airstream direction

y distance in the transverse direction

ρ density

μ molecular viscosity

Chapter 1

INTRODUCTION

A liquid's injection into a quiescent atmosphere is used widely in internal combustion applications as well as fabric weaving industries. The internal geometry of a nozzle determines its application. Longer, continuous liquid jets are required in hydroentangling processes so that any form of atomization of the liquid jet is detrimental. On the other hand, atomization of the liquid jet is required in internal combustion systems to permit more complete combustion. These last applications can be extended to the combustion of fuel in scramjets and ramjets in the presence of a crossflow. Due to environmental concerns, there have been continuous improvements in direct injection, diesel engines for higher combustion efficiencies and lower exhaust emissions. Accordingly, the liquid jet spray and flow characteristics formed by a fuel injector geometry have been a primary research focus. Indeed, determining the characteristics of fuel flowing through an injector nozzle is one of the most active investigation areas. This activity suggests that the geometry of a nozzle is very important factor in a jet's atomization.

The transverse injection of a liquid jet into a subsonic crossflow is encountered commonly in liquid rocket engines, air-breathing propulsion systems, injection of cooling sprays for turbine blades and fuel in afterburners, as well as agricultural sprays. The most important engineering parameter in all these applications is the jet's penetration and breakup length as a requirement for the efficient mixing of air and fuel. High temperatures and pressures are employed in combustion chambers of modern aircraft engines to fulfill high thrust requirements. A by-product is an escalating production of pollutants like NO_x. The emission of pollutants from gas turbine engines has been of

great environmental concern for several decades. Emissions in the form of carbon monoxide, nitrogen oxide, sulphur oxide and unburned hydrocarbons are released into the atmosphere [64]. Liquid injection into a crossflow has been one of the new developments in curbing excessive emission of pollutants as well as increasing combustion efficiency. Then the main concept is to quash stoichiometric reactions [64].

The present focus is the generation of fine droplets of liquid which are entrained in a crossflow of air before entering a combustion chamber. The conventional procedure is to inject just the liquid jet at a very high pressure. To achieve maximum penetration, the injection pressure should be as large as practically feasible. Hence, aerated liquid jets have been introduced. They produce smaller drops in a crossflow that have higher velocities at lower injection pressures than those of conventional jets. Moreover, they have a higher trajectory/penetration height due to a greater momentum-flux ratio, q. An effective mixing of the air fuel mixture is achieved if the atomization of the liquid into fine droplets and the spray is distributed precisely in the crossflow. During atomization of the liquid jet, the smaller drop diameters generated increase the surface area of the liquid jet and, hence, a higher rate of mixing is achieved. Then the dynamics of the liquid jet upon contacting the crossflow of air becomes vital due to its effect on the combustion. From various research [19, 21, 24], the liquid jet in an air crossflow has been divided into three regimes, namely (i) the column of the liquid jet (ii) ligament and (iii) droplet. Upon interacting with the crossflow the liquid jet would be in one of these three regimes or it would exhibits two of these regime properties. For example, the spray properties are influenced by a nozzle's internal flow, turbulence at the exit of a nozzle or the velocity profile of the jet.

Co-axial liquid jets injected into a subsonic air crossflow have been mostly researched in comparison to the transverse injection of a liquid jet in a subsonic cross airflow. However the expectation of having generally better combustion has led to a fair number of studies involving liquid jets in a subsonic cross airflow. Such applications have been evident in the areas of combustion, cooling of turbine blades and reacting gases, propulsion systems, coatings, etc. Although an unbroken liquid jet with great momentum is desired in liquid jet cutting applications and hydroentangling processes, an atomized liquid is preferred in combustion. The greater prominence of ramjets and scramjets has heightened further interest in studying liquid jets injected into a crossflow. Studies have been launched into the role played by liquid jet's properties, such as surface tension, viscosity etc. on the breakup processes of the liquid jet. In all these applications, much attention has been devoted to the atomization of the liquid jet, but progress has been inhibited by the complexity of phenomena such as cavitation and hydraulic flip. Atomization processes for a turbulent liquid jet are substantially different from those of non-turbulent liquid jets. However, the differences may be insignificant when external factors, such as aerodynamic drag from the subsonic crossflow, are very notable. These phenomena compete more often than not, for dominance as the operating conditions vary. The general objective of researching a liquid jet in a crossflow is to achieve an appropriate mixing of the liquid jet and the crossflow that would result in an efficient combustion as well as a massive reduction in the production of NO_x after the combustion. Therefore, great emphasis is placed on efficient ways of generating fine droplets and, simultaneously, having the liquid jet penetrates farther into the crossflow at relatively lower injection pressures.

Recent developments in combustion systems, as well as the existence of numerous types of injector nozzles, emphasize the need to better understand the effects of a nozzle's geometry on the occurrence of cavitation and hydraulic flip, as well as on a liquid jet's trajectory and breakup length. It is known that the fuel injection system of a combustor or an engine is of primary importance in increasing the combustion efficiency as well as reducing environmental pollution. This suggests that the spray structure and penetration, which ensure efficient fuel-air mixing within the combustor, are determined by the injector nozzle's geometry as well as injection conditions [54]. The main reason for exploring other types of nozzle geometries is to enhance the atomization as well as attain efficient fuel/air mixing at lower operating pressures for potentially cleaner air. One other application which relies heavily on the nozzle geometry is fabric weaving. This application requires a long continuous jet so that the nozzle's design should avoid irregularities that would promote atomization. The geometry of the injector nozzle clearly plays a vital role in achieving the desired objective. It is in the context of these applications that a study of a nozzle's geometry is appropriate. Indeed, varying an injector nozzle's geometry influences the internal flow of the liquid jet and could enhance atomization, cavitation or hydraulic flip within the nozzle.

Experimental data for a cavitating flow of a liquid jet in a quiescent atmosphere abounds in the open literature. However much work still need to be done for a subsonic crossflow because previous results cannot be extrapolated directly. Therefore there is a compelling reason to study effect of a nozzle's geometry on the liquid jet emitted in a subsonic crossflow particularly when there is cavitation or a hydraulic flip. Therefore the initial aspect of this study is:

1. To investigate the effects of a nozzle's geometry on the breakup length of a water jet as well as the occurrence of cavitation and hydraulic flip in a quiescent atmosphere.

After establishing the occurrence of cavitation and hydraulic from a quiescent atmosphere experiment, a subsonic crossflow of air needs to be introduced to study its effect and those of a nozzle's geometry on the water jet's breakup length and trajectory. Therefore, the second aspect of the experiments is:

2. To study the effect of cavitation and hydraulic flip on the breakup length and trajectory of the liquid jet in a subsonic crossflow.

It is believed that the results of the present investigation should considerably improve knowledge about a water column's trajectory in a subsonic cross airflow in the presence of cavitation and hydraulic flip. Also, the understanding of the effect of a nozzle's geometry on a liquid jet's trajectory should give a better overall perspective.

Chapter 2

LITERATURE REVIEW

The perpendicular injection of a liquid jet into a crossflow and its subsequent atomization into fine droplets by aerodynamic forces has several combustion applications, which include ramjets, scramjets and gas turbine engines. This configuration was found to help in reducing combustion temperatures [1, 2] and improving fuel-air mixing [3, 4], which, in turn, leads to a more efficient combustion with less pollutants emissions [1-6]. Liquid injection into a quiescent atmosphere and its breakup mechanisms have also received considerable attentions due mainly to 1) understanding the breakup of a liquid jet is a prerequisite for understanding liquid injection in a crossflow, and 2) the fact that a liquid jet is also employed in the nonwoven industries to replace steel needles used in such applications where high speed water jets with long breakup lengths are required to develop a technique for entangling fibres in a loose web (e.g.[7]).

The breakup mechanism of water jet through a nozzle has been extensively studied both theoretically and experimentally. It was reported that the liquid jet's breakup behaviour can be affected by several factors, such as hydrodynamic forces (viscous forces, surface tension and initial disturbance) [8], aerodynamic forces [9, 10], liquid jet turbulence [11, 12, 13], the jet's exit velocity profile effect [14], liquid jet vibration [12, 13], cavitation and flow separation within the injector nozzle [12, 13, 26]. For instance, Ng et al. [15] observed a smooth jet with no initialization of surface breakup even at very high jet Reynolds number (Re = 30,000). This behaviour persisted over the observable length of the liquid jet (up to $75d_j$) which is believed to be an evidence that the primary breakup process of a round non-turbulent liquid jet in a crossflow is not due to the initial

disturbances within the liquid jet but rather due to the aerodynamic effects of the crossflow.

Sallam et al. [16] observed two mechanisms for ligament breakup for a turbulent liquid jet in quiescent atmosphere: (a) ligament tip (Rayleigh) breakup and (b) ligament base breakup. Wu et al. [17] in a review reported that there was no droplet generation of a fully developed turbulent liquid jet in a quiescent atmosphere until the onset of breakup. In these situations, liquid jet breakup is solely controlled by the jet turbulence and the breakup locations depend only on the Weber number of the liquid jet [17]. In a recent publication, Birouk and Lekic [18] reviewed extensively liquid jet breakup mechanisms in quiescent atmosphere. The primary breakup properties of a liquid jet in subsonic crossflow have also been studied extensively. Both Wu et al. [19] and Vich et al. [20] reported similarities between the breakup properties of round liquid jets in crossflows as well as the secondary breakup of the drops. Wu et al. [19] observed that the liquid jet injected into a crossflow underwent bag, multimode and shear breakup. The bags are membranes formed by thin jets exposed to high aerodynamic drag forces [41]. Vich et al. [20] determined breakup regimes for bag and liquid column breakup which were somehow different than those of [19]. Nonetheless, both studies indicate that the presence of liquid jet distortion [19] or effects of turbulent transition on the liquid jet's breakup trend [20] are caused by disturbances from within the nozzle. Mazallon et al. [21] in an experiment identified four breakup regimes which are: (i) liquid-column breakup, (ii) bag breakup, (iii) bag/shear breakup, and (iv) shear breakup. The point where the liquid column breaks up into ligaments represents the jet's column breakup . It is to be noted that the variations in the different modes of breakup greatly depends on the crossflow

Weber number. Sallam et al. [17] identified that the breakup of the liquid column occurred when the amplitudes of liquid surface disturbances at the jet exit grow to the point where they reach the liquid jet axis. It was found that the density of the surrounding gas has a great effect on the mode of the liquid jet breakup [22, 23].

The dynamic pressure of the crossflow causes the liquid jet to flatten and this makes it bend in the direction of the air [19, 24, 25, 26]. After bending, the liquid jet first undergoes surface breakup to form ligaments and droplets and then subsequently surface waves appear on the liquid column [19]. It was also observed that the location of the liquid jet's breakup coincides with one of the troughs of the windward surface waves on the liquid column [19]. Atomization of the liquid jet was described by Ingebo et al. [27] as the process of forming ligaments from the crests of the waves that form on the surface of the liquid jet. These waves were considered to be responsible for the breakup of the liquid jet [2]. Gutmark et al. [28] reported that vortex structures formed with the liquid jet upon interacting with the crossflow might be responsible for the surface undulation of the liquid jet. Ahn et al. [29] purported that when liquid is injected into crossflow, acceleration waves grow on the surface of the liquid column thereby leading to the deformation of the liquid column and subsequent flattening due to the aerodynamic drag force. Upon flattening, the liquid column further disintegrates into ligaments and droplets.

Most published studies on liquid jet breakup in a crossflow focused on the jet column's breakup and trajectory where the effects of, for example, liquid properties [30], turbulent nature of the jet [31], and nozzle geometry [19, 32, 33] (i.e., which leads to cavitation and hydraulic flip) were examined. Generally, the spray plume can be divided into three

regions, namely, the liquid column, ligament and droplet regions [6]. In other applications, where cavitation prevails, the corresponding three regions are termed non-cavitating, cavitating and hydraulic flip regimes, which is the detachment of the liquid jet from the internal surface of the nozzle [11]. The liquid column's breakup length and trajectory determine the location of the onset of these droplets. Events leading to the primary breakup of a liquid jet are important since they initiate atomization processes. These parameters are very useful in the design of injectors as well combustors for optimum combustion efficiency [29]. However, no relation has yet been established or observed between the jet's breakup mechanisms, nozzle's internal flow (cavitation and hydraulic flip) and the geometry of the nozzle.

Liquid jet's penetration depth was defined by Schetz et al. [34] as an asymptotic value measured at 6.25 jet diameters downstream of the center of the injector nozzle. It was expressed as a function of the injector's diameter and the liquid jet's/freestream dynamic pressure ratio. They found the jet's maximum trajectory to be the distance required to redirect the jets momentum in the direction of the crossflow. Several attempts have been made to either model or predict the liquid jet's behaviour transversely injected into a subsonic crossflow. Three main forms of liquid jet trajectory correlations have been reported in the literature, an exponential function [35], a logarithmic function [36], and a power law [19, 29, 30, 37]. Inamura [25] deduced a semi theoretical equation to simplify the liquid jet's trajectory in subsonic crossflow and this was compared with the jet's penetration measurements. Chen et al. [35] proposed a complex three-term exponential correlation for the liquid jet's trajectory in a high subsonic crossflow. Wu et al [6, 19] developed two different correlations for the liquid column and droplet regions in subsonic

crossflows by assuming that the liquid acceleration balances the aerodynamic drag forces in the cross stream direction. These assumptions were confirmed through experiments. Schetz et al. [38] noted that the growth of these acceleration waves on the liquid column by the crossflow's aerodynamic drag force play a major role in the jet's breakup processes. It was observed by Wu et al. [9] that both the jet's surface breakup process and that of the liquid column occurred at large liquid jet momentum. They solved the jet's column fracture utilizing the time scale for aerodynamic secondary breakup of the droplets and concluded that the liquid column always broke at a distance of 8.06 ± 1.46 jet diameters downstream of the nozzle. It was also reported by Inamura et al. [39] that the breakup distance in the cross stream direction was insensitive to the liquid/air momentum flux ratio as well as the properties of the liquid jet. The water jet's trajectory in a subsonic crossflow was investigated by Iyogun et al. [37] for a streamwise distance up to $x/d < 12$. The data agreed with most published correlations but the agreement deteriorated further downstream (i.e. $x/d \geq 60$) in comparison to the results of Chen et al. [35]. Several empirical correlations have been reported on the jet's penetration and width [19, 29, 30, 35, 36, 37].

It was reported that surface tension and viscosity does not play a major role in the liquid columns trajectory and breakup length (e.g., [21, 39]). Nejad and Schetz [40] observed that, for less viscous liquid jets with a correspondingly low surface tension, the jet's breakup and atomization is due to the formation of waves along the surface of the liquid column. On the other hand, they reported that ligament formation is the principal mechanism for the jet's breakup and atomization for a high viscosity liquid jet. For example, it was observed by Nejad and Schetz [40] that, for very high viscosity liquid at

low values of q, the jet breaks into ligaments rather than droplets. However, even for the very high viscosity liquids (viscosities much higher than that of water), Nejad and Schetz [40] observed that at high q, the jet breaks up into droplets. Birouk et al. [41] proposed two correlations to determine both the transverse and streamwise penetrations of viscous liquid jets before breakup. The breakup locations they found for low viscosity liquid jets (viscosities comparable to that of water jet) agreed well with those of Wu et al. [19]. Conversely, for more viscous liquid jets, both the transverse and streamwise penetrations differed from the data of Wu et al. [19].Birouk et al. [30], however, reported that the liquid jet's viscosity played a less significant role in the trajectory of liquid jet in a subsonic crossflow.

In addition to the liquid properties and aerodynamic forces, nozzle's geometry has also found to impact the jet breakup phenomenon [11, 29, 32, 42]. Begenir et al. [7] observed flow through three different nozzles (i.e. cone-up, cone-down and cylindrical) and reported that flow through cone-up nozzle configuration generated liquid columns with shorter breakup lengths compared to nozzles with cone-down configuration. This was attributed to the occurrence of cavitation. Ghassemieh et al. [43] reported that increasing nozzle diameter from 120 to 170 μm produced liquid jets governed by inertia forces, viscous forces and cavitation effects. Nozzle surface roughness critically affects some of the important factors that control flow characteristics [43]. New et al. [44] utilized LIF technique to experimentally determine flow structures in a water tunnel for elliptic nozzles with aspect ratios in the range of 0.3 – 3. Two adjacent counter vortex pair was observed for nozzles with low aspect ratio. Whereas only one counter vortex pair was seen for nozzles with high aspect ratios. Studies by Liscinsky et al. [45] on jet's

penetration and mixing in a crossflow by utilizing circular and non-circular nozzles (square, elliptical and rectangular) revealed minimal change in mixing for all the noncircular nozzles. Gutmark et al. [28] studied flow through circular and noncircular nozzles in a crossflow and reported that the boundary layer as well as the nozzle geometry was very important in determining evolution of the jet in crossflow. It was observed that a non-turbulent liquid jet was produced by a super-cavitating nozzle [15]. Osta et al. [33] observed flow through nozzles with various L/d in a subsonic crossflow and reported that increasing L/d produces a turbulent liquid jet.

The cavitation and hydraulic flip phenomena and their interplay with nozzle geometry were found to significantly impact the liquid breakup mechanisms [46, 47, 48, 49, 50, 51, 52, 53]. For example, Ahn et al. [29] reported lower liquid jet trajectories at the inception of cavitation and hydraulic flip. Song et al. [32], in a similar experiment to that of Ahn et al. [29] developed a correlation for the trajectory of a non-cavitating liquid jet in a cross flow. Their results had a good agreement with that published by Wu et al. [19] but only at lower momentum flux ratios, q. They also observed that under cavitation conditions, shorter column trajectories were measured in crossflow [32]. It has also been reported by Tamaki et al. [12, 13], Suh et al. [53], Park et al. [42], Wu et al. [31] and Chang et al. [54] that atomization of the liquid jet depends greatly on the disturbance caused within the liquid jet by cavitation within the nozzle, inner surface roughness of the nozzle and the turbulent nature of the jet. Tamaki et al. [12] observed that atomization of the liquid jet was greatly enhanced when the liquid jet was disturbed by the collapse of cavitation bubbles within the orifice which resulted in shorter liquid column breakup lengths.

As briefly discussed above, extensive research has been conducted into the interaction of a liquid jet with its ambient, whether a quiescent or a crossflow environment. However, published literature reveals that although significant progress has been made, there is still a lack of knowledge of certain aspects on a liquid jet breakup in a crossflow. A good example is the extent of the impact of the geometry of a nozzle, and more specifically in the presence of cavitation and hydraulic flip phenomena. Relatively limited pertinent studies have shown how the geometry of a nozzle can alter the ensuing liquid jet behaviour. Faeth et al. [55], Tseng et al. [56, 57] and Ahn et al. [29] all observed that rounding the internal edges of a nozzle's orifice can generate a more steady liquid jet and hence a longer column length of the liquid jet. Tamaki et al. [12, 13], however, observed shorter liquid jet breakup columns in a quiescent atmosphere when a wire was placed inside the nozzle to promote cavitation. They also observed that increasing the nozzle's L/d eliminates the occurrence of hydraulic flip, which was in agreement with the conclusion of Ahn et al. [29]. Both these studies [12-13] reported that longer liquid jet breakup lengths in the presence of hydraulic. It was also demonstrated that an increase in nozzle's L/d eliminates the occurrence of hydraulic flip; whereas turbulent liquid jets are generated for flow through nozzles with longer L/d [33]. The effect of nozzle's contraction angle is still relatively unknown, especially in crossflow configuration, where most of the work conducted in this field was in quiescent atmosphere [43, 58]. Moreover, there are limited studies on how the internal surface roughness of a nozzle affects the liquid jet [54]. The focus of the present study is on the effect of nozzle geometry where there is less established knowledge (e.g. Birouk and Lekic [18]). Therefore, the present study is an attempt to fill this gap by examining thoroughly nozzle's geometry parameters

on a water jet column breakup and trajectory in a cross flow. These parameters include contraction angle, nozzle's orifice length to diameter L/d, nominal surface roughness, and diameter.

Chapter 3

EXPERIMENTAL FACILITY, INTRUMENTATION AND METHODS

The experimental facility consists of a subsonic wind tunnel and a liquid injection system. The associated instrumentation includes: a seeding particle generator, a laser Doppler velocimetry (LDV), a high-speed CCD camera and pressure gauges. A brief description of all the different components is presented next.

3.1 Experimental Facility

3.1.1 *Wind Tunnel*

The wind tunnel delivers a wide range of airflow speeds with an invariably low turbulence intensity of about 1% in the test section. It is an open loop, subsonic type (see Fig. 3.1) that operates at atmospheric pressure.

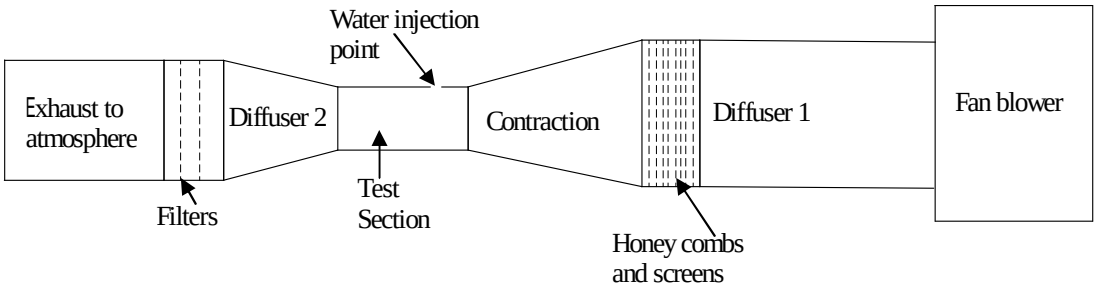

Figure 3.1. Schematic of the wind tunnel.

Air is ingested into the tunnel by means of a blower after which it goes through a diffuser. At the exit of the diffuser, the air flow passes through a set of conditioning screens and honeycombs in the settling chamber. Then, the air is accelerated through a contraction section after which it goes through the square test section. The sides of the test section are a transparent acrylic for easy visualization. Sets of screens are installed

after the test section to filter the air before it is released into the atmosphere. The wind tunnel is controlled by using an H7, True Torque Control, Adjustable Speed Drive for the blower so that the cross airflow speed in the test section can be varied between 12 to 71 *m/s*.

The main components of the wind tunnel are described next.

a. *Blower section*: The blower is a Northern Blower, Winnipeg, centrifugal fan having airfoil type impellers. It has a motor capacity of 25 HP. An H7 Adjustable Speed Drive (ASD), which is a product of TOSHIBA, is used to drive the fan. The H7 True Torque Control, Adjustable Speed Drive is a standard-duty, solid-state AC drive that has True Torque Control. It uses digitally controlled, pulse width modulation. There is an easy-to-read, 240 × 64 pixel, graphical LCD screen with a user-friendly Electronic Operator Interface (EOI) that is used primarily to control the wind tunnel operations, particularly the speed drive of the blower.

b. *Diffuser*: Two diffusers are used in the wind tunnel. The first diffuser is placed between the fan blower and the contraction section. The first diffuser is made of fibreglass and has inlet and outlet dimensions of 718 *mm* × 543 *mm* and 762 *mm* × 762 *mm*, respectively, with a total length of about 1.7 *m* to diffuse the airflow prior to the settling chamber and prevent flow separation. The second diffuser is used to diffuse the airflow downstream of the test section and, hence, it slows the airflow in order to reduce power consumption. It is made of aluminum sheets and has inlet and outlet dimensions of 400 *mm* × 400 *mm* and 1170 *mm* × 700 *mm*, respectively, with a length 2.9 *m*. This diffuser accommodates a series of filters to filter substrates from the cross airflow before it exits into the atmosphere. A valve is fixed at the

bottom of the second diffuser, just in front of the filters, to drain water that has collected and settled.

c. *Settling Chamber*: The settling chamber separates the first diffuser and the contraction section. It consists of honeycombs, followed by series of flow conditioning screens. The honeycombs are positioned in the settling chamber just before the contraction section to remove swirl and lateral, mean velocity variations. The conditioning screens are used to improve the uniformity of the cross airflow. The settling chamber has inlet and outlet dimensions of 762 *mm* × 762 *mm* and 762 *mm* × 762 *mm*, respectively, and runs a length of about 400 *mm*. Its outer surfaces are aluminum sheets.

d. *Contraction section*: The contraction section's main purpose is to increase the airflow's speed immediately before the test section. The contraction is made of fibreglass and it has inlet and exit dimensions of 762 *mm* × 762 *mm* and 305 *mm* × 305 *mm*, respectively, with a length of 940 mm long [59].

e. *Test Section*: The test section has a 300 *mm* square cross section and a 600 *mm* length. It is made of acrylic to facilitate flow visualization and laser diagnostics.

3.1.2 Liquid Injection System

A liquid injection system was designed to deliver water jet into a quiescent atmosphere and, later, into a subsonic cross airflow. The injection system is composed mainly of a pressurized liquid chamber, injector nozzles, compressed nitrogen tank, pressure gauges and a set of stainless steel pipes and valves. It is shown schematically in Figure 3.2.

The volume flow rate of the water jet is controlled by regulating the compressed nitrogen's pressure in the pressurized liquid chamber. Liquid jets are injected vertically

downwards into either a quiescent atmosphere or a subsonic cross airflow from a nozzle whose exit is flush with the inside of the test section top surface. The pressure inside the chamber is controlled by using a digital pressure gauge whose working range is between 10 *psig* and 80 *psig*. The resulting speed of the water jet is between 9 *m/s* and 30 *m/s* at the nozzle's exit. This speed range is obtained by using seven identical nozzles having different diameters of 1 *mm* and 2*mm*. It is to be noted that, for the crossflow experiments the nozzle is positioned 200 *mm* downstream of the test section's inlet. The main components of the liquid injection system are described briefly next.

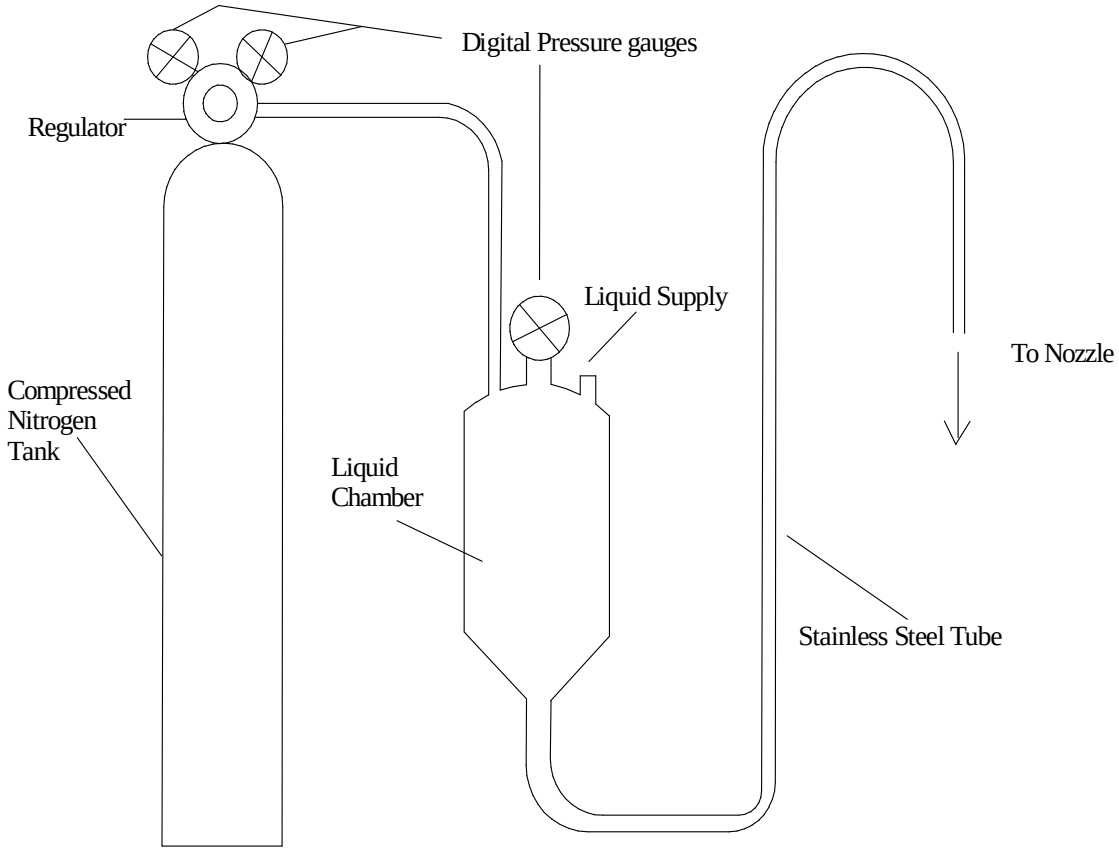

Figure 3.2. Schematic of the water injection system.

3.1.2.1 Pressure Chamber

The stainless steel pressure chamber is the main component of the liquid injection system [59]. Water is stored here before it is forced through a nozzle. The pressurised water chamber is made of 12 inches of 6-inch inner diameter pipe, with a 6-inch cap on top and a 6:3 *inch* cone reducer followed by a 3-inch cap on the bottom. The cone reducer is included to reduce turbulence at the exit. There is a 1/2-inch NPT port on the top surface of the pressure chamber, to fill the chamber with any injectant, as well as a 1/4-*inch* and 3/8 *inch* NPT fitting for the pressure gauge and nitrogen line respectively, Moreover there is a single 3/8-*inch* NPT fitting situated on the bottom of the chamber to eject the stored water. A steel baffle plate is located inside the chamber, beneath the nitrogen line, to prevent the nitrogen from touching the water. The chamber was heated initially to more than 1000 *ºC* for an hour to allow chromium, which could cause rusting, to dissolve. The chamber is then pickled and pacified to make the chamber inert [59].

3.1.2.2 Pressure Gauge

The pressure gauges are very important in controlling the water jet's exit speed from a nozzle. Two gauges having different sensitivities are used. One has a range of 0-100 *psig* and the other goes up to 500 *psig*. Absolute Process Instruments Inc. supplied both gauges. The 500 *psig* gauge is accurate to 0.25% while the 100 *psig* gauge is accurate to 0.1%. The gauges, which are both supplied with a 1/4 NPT fitting, are plastic coated to give them additional corrosion resistance. This is important as one of the gauges is situated near the funnel used to fill the chamber with the test liquid (water). The gauges have a double overpressure rating (i.e. the gauge is damaged when exposed to twice its maximum design pressure) and a quadruple burst rating.

3.1.2.3 Nozzles

Different nozzles are used that have two different diameters and various internal parameters. They are employed hereto inject water into a quiescent atmosphere or a subsonic cross airflow. Also, the transition from the nozzle's tapered section to its straight exit section is not rounded in order to study the effect of cavitation. Figure 3.3 shows a schematic of the nozzles. Seven injector nozzles are utilized; six have an exit diameter of 2 *mm* and the remaining nozzle designated N2 has an exit diameter of 1 *mm*. Their parameters and designations are given in Table 3.2 and Figure 3.3. All the nozzles have sharp edges to permit the generation of a turbulent jet at each nozzle exit. The nozzle's internal surface roughness was specified by the manufacturer (Bristol Aerospace Ltd).

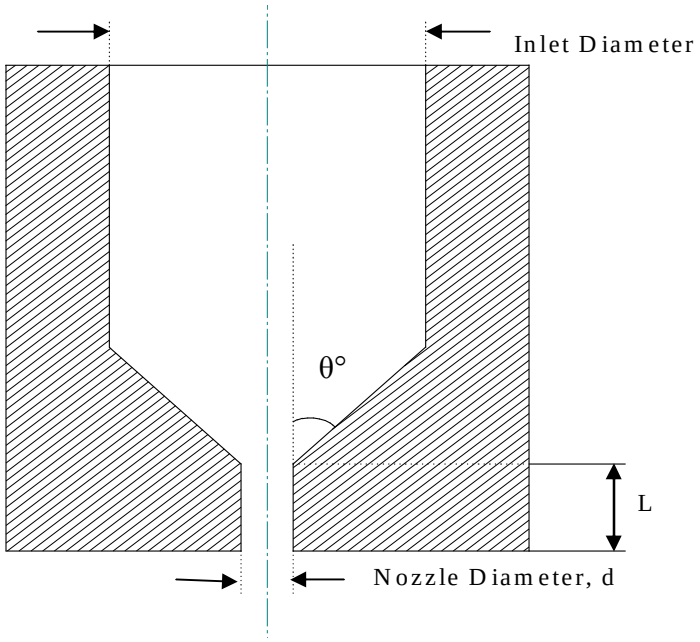

Figure 3.3. Schematic of a typical injector nozzle.

3.2 Instrumentation

The measuring devices used to characterize the subsonic crossflow are described now.

3.2.1 Seeding Particle Generator

Two10-bar LaVision droplet generators produce micro-sized bis (2-ethylhexyl) sebacate, 95% drops to seed the cross airflow in order to characterize it. The drop's diameter range between 0.2 μm to 1.0 μm and faithfully follow the airflow. The seeders are positioned at the blower section air intake.

3.2.2 Laser Doppler Velocimetry (LDV)

The Laser Doppler velocimetry's main components are illustrated in Figure 3.4. They enable the velocity of the subsonic crossflow to be measured non-intrusively. The operating principle of the LDV is described next.

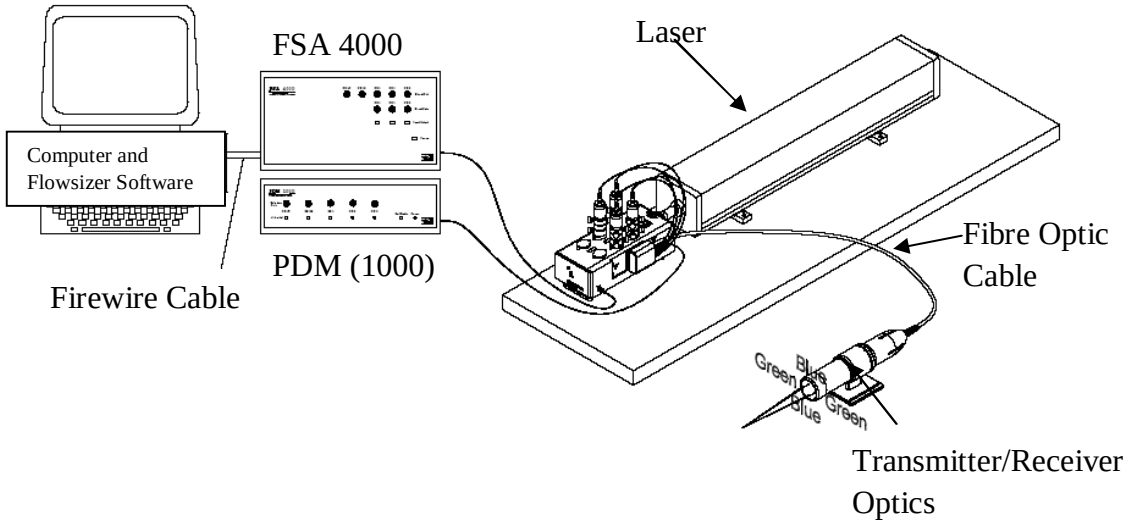

Figure 3.4. Schematic of LDV technique [59].

3.2.2.1 Operating Principle of the Laser Doppler Velocimetry (LDV)

The Laser Doppler Velocimeter measures the velocity of the flow tracers from the particle generator. The two dimensional LDV measurement technique uses an InnovaI -

70C– 5 series, 5 W, continuous wave argon-ion type laser to generate a coherent light beam to illuminate the flow seeders. This generates two green and two blue beams having an equal intensity and wavelengths of 514.5 and 488 *nm*, respectively. All four beams are transmitted through optical fibre cables into the transmitting system that uses a 350 *mm* focal length lens to intersect the beams. The intersection at the focal point of the lens forms a probe volume. This volume consists of a set of bright and dark fringes. A particle scatters light as it crosses the bright fringes. The scattered light is collected by receiving optics and converted to proportional electrical signals by using Photomultiplier Tubes (PMTs). The Photo Detector Module, (PDM 1000) sends an electrical signal to the TSI Flow Size Analyzer's 4000 (FSA 4000) processor. The latter extracts the frequency at which the seeding particle crosses a bright fringe. This frequency is known as the Doppler frequency, f_D. As the fringe spacing, δ_f, is fixed geometrically, the Flowsizer can determine the particle's velocity, u_∞, from

$$u_\infty = \delta_f f_D. \qquad (3.1)$$

Then turbulence data and mean-velocities can be calculated after twenty five thousand (25,000) particles have crossed the probe volume.

3.2.3 High Speed Digital Imaging

A 12-bit, high resolution digital camera from Dantec Dynamic NanoSense4M camera, coupled with a charge-coupled device (CCD) having 1024 x 1280 pixels, is used to image the dynamics of the water jet's breakup and trajectory. The pixel pitch of the camera is 7.4 μm. Measurements are made for a flow field size of 71 x 56 *mm*. The camera has a changeable frame rate between 60 and 8,000 fps, a zoom lens of 5 to 105 *mm* with a magnification of 1.8 and a maximum shutter speed of 6.25 μs. The imaging system stores

captured images in an Image Memory on the Controller Unit. The components of the Dantec Dynamic NanoSense4M camera are the: (*i*) lens, (*ii*) CCD chip, (*iii*) shutter, and (*iv*) trigger switch. Images can be viewed in a forward or reverse mode at selectable frame rates from 1 to 8,000 frames per second, with a frame-by-frame mode or a freeze frame mode. A sequence or part of a sequence can be saved in a computer file on a computer disk or a removable storage media for later retrieval. All the settings of the camera (frame rates, record rates, frame storage, recording, etc) are adjusted through Motion Pro software installed on the computer connected to the camera. A stroboscope is used to backlight the flow field and obtain a good contrast and better illumination.

3.3 Experimental Methods

3.3.1 Experimental Procedure in Quiescent Atmosphere

The setup is designed carefully to eliminate extraneous building vibrations that could contribute immensely to the generation of a turbulent jet. This was done by sturdily fixing the entire tubing system to the concrete wall of the lab. The entire setup comprises compressed nitrogen stored in a cylinder and a 9-liter, stainless steel water container connected to the top of the pressurized nitrogen by using stainless steel tubes. Water from the tank is pressurized by the compressed nitrogen for sixteen operating pressures between 0.136 and 0.653 *MPa*. The pressurized water is discharged through the nozzles into the atmosphere and then images are captured at a nozzle's exit to study a jet's breakup length.

3.3.2 Experimental Procedure in Subsonic Crossflow

After conducting the experiment in a quiescent atmosphere, the whole setup is moved into the wind tunnel in order to introduce a subsonic cross airflow. Upon filling the

pressurized chamber with water, the H7 adjustable fan drive is turned on and set to the required fan speed drive. Once the wind tunnel is operating, the required water jet is set by opening the nitrogen tank valve and adjusting the pressure delivered to the chamber by means of a regulator. (Also see the nozzle's calibration presented more conveniently in the next chapter). Once the pressure stabilizes at the pressure gauge on the pressure chamber, the valve connections on the stainless tubing are opened to deliver water through the nozzle and into the subsonic cross airflow.

In both quiescent atmosphere and subsonic crossflow procedures, the imaging system is positioned to capture the water jet's breakup length, trajectory and the breakup processes itself. As mentioned earlier, the flow field is illuminated by a stroboscope. Once the images have been captured, they are saved in a *JPEG* format. Two hundred images are saved for each set conditions, and processed to determine the breakup length of the water jet in a quiescent atmosphere, although preliminary experiments demonstrated that even less number of images (<200) can still provide the same results. To determine the water column's breakup length and trajectory in a subsonic crossflow, fifty images were found sufficient. A MATLAB code given in Appendix A was used to compute the water jet's breakup length in both quiescent atmosphere and subsonic crossflow, as well as its trajectory. The code averages fifty and two hundred images in a crossflow and quiescent atmosphere, respectively, to calculate an average value for every x and y position of the water jet. Figure 3.5 defines the fixed xy coordinate frame and shows a schematic of the experimental arrangement. It was assumed that variations in the z-direction are negligible. Table 3.1 gives a summary of the experimental conditions used.

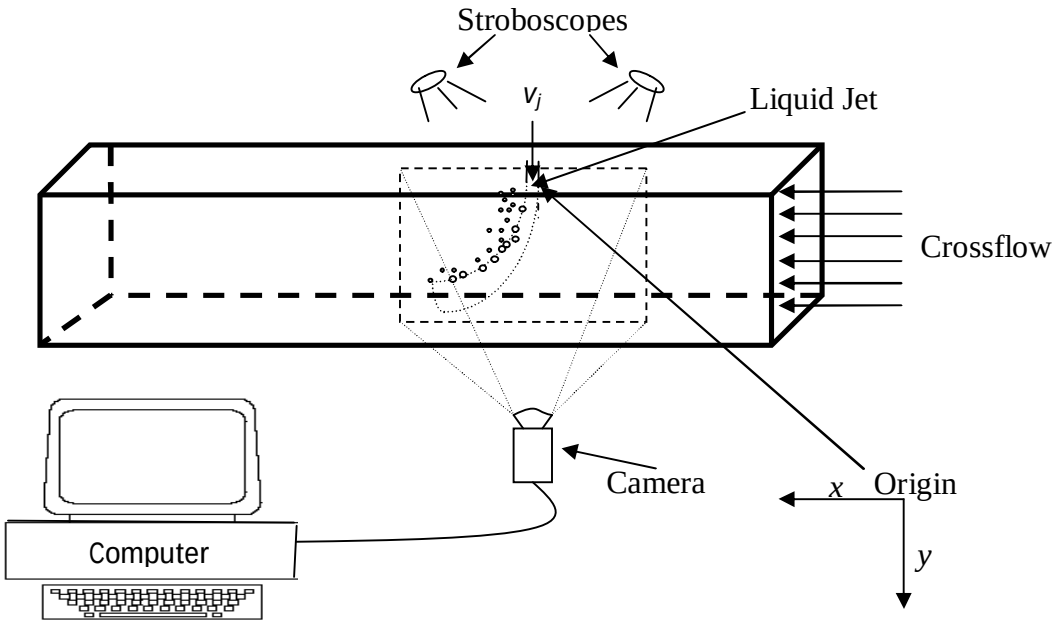

Figure 3.5. Schematic of experimental setup.

Table 3.1. Experimental conditions.

Parameter	**Value**
Cross air flow speed, *m/s*	23.6-70.8
Water jet speed, v_j, *m/s*	5-30
Nozzle diameter, *d, mm*	1, 2
Momentum flux ratio, *q*	5.76-124
Pressure, *MPa*	0.136 – 0.653
Nozzle L/d ratio	4, 6, 10
Liquid Injectant	Water

Table 3.2. Nozzle Parameter.

Geometric parameters	**Nozzle identification**						
	N2	N3	N4	N5	N6	N7	N8
Diameter (*mm*)	1	2	2	2	2	2	2
Contraction angle (°)	30	30	45	45	60	45	45
Nominal Surface roughness (μm)	6.35	6.35	6.35	3.18	6.35	3.18	3.18
L/d	4	4	4	4	4	6	10

Chapter 4

NOZZLE CALIBRATION AND CHARACTERIZATION OF CROSS AIRFLOW

The seven nozzles used experimentally were calibrated to determine the water jet's exit speeds at the different operating pressures. The airflow in the wind tunnel's test section was also investigated to determine its mean velocity and turbulence intensity profiles. This chapter details the nozzles' calibration and describes the crossflow.

4.1 Calibration of Nozzles

The inlet to the pressure chamber is connected directly to a tap. Nine (9) litres of water is allowed into the chamber through the connecting hose. The bleed valve is kept open to allow any trapped gases to be vented from the pressurized chamber so that the filling process is sped up without generating air bubbles. The connecting valve between the chamber and the tap source is shut once the water chamber is filled. Then the bleed valve is closed to prevent leaking after which nitrogen is allowed into the pressure chamber. The valve controlling the compressed nitrogen tank is opened fully with its regulator closed. The knob on the regulator is opened slowly to increase the pressure which is read on the highly accurate digital pressure gauge mounted on top of the pressure chamber. Upon meeting the required pressure, a valve on the stainless steel tubing supply, which connects the bottom of the chamber to the nozzle, is opened to allow water to flow into the nozzle. The nozzle is calibrated by measuring the water jet's exit speed from the nozzle. When the water runs fully out of the pressure chamber, the nitrogen tank is closed and the system is vented to room pressure and refilled so that it is always full at the start of a test. If part of the water remains in the pressure chamber after completing a test, the bleed valve is used (after the tank is shut off) to vent the chamber pressure so that it

reaches to room pressure. An alternative procedure having the same result is to close the valve located immediately after the regulator instead of closing the nitrogen tank. This last procedure allows the chamber to be refilled and recompressed quickly to a given set pressure.

All seven nozzles were calibrated. The digital pressure gauge mounted on top of the pressure chamber displayed only the pressure within the chamber, not the speed or volumetric flow rate of the water jet. Consequently, the speed at which the water leaves the nozzle was determined indirectly. This procedure involved running the apparatus at different given pressures (as described above) and collecting the volume of water discharged from the nozzle into a calibrated beaker (with an accuracy of ±5 ml) over a period measured with an electronic timer having an accuracy of ±0.001 seconds. Knowing the nozzle exit's cross sectional area, *A*, the volume of water collected, *V*, and the discharge time, *t*, the jet velocity, v_j, is determined as follows. First the volumetric flow rate, $\dot{Q}$, is derived from

$$\dot{Q} = \frac{V}{t} = Av_j \qquad (4.1)$$

where $A = \frac{\pi}{4}d^2$ is the cross sectional area of the nozzle whose internal diameter is *d*. Substituting the expression for *A* into Equation (4.1) yields,

$$v_j = \frac{4V}{\pi d^2 t} \qquad (4.2)$$

Three separate measurements were taken for all the nozzles at each pressure in order to check the experiment's repeatability. The arithmetic average of the three measured velocities was calculated and used for a given set pressure. This procedure was repeated

over the operating pressures range extending from 0.136 to 0.653*MPa*in increments of 0.0347 *MPa*. The uncertainty of the measured jet speed was ± 0.4 *m/s*.. Figure 4.1 shows the water jet's speed through two nozzles that had diameters, *d*, of 1 and 2 *mm*. The figure indicates that the velocity of the water jet increases with a greater injection pressure.

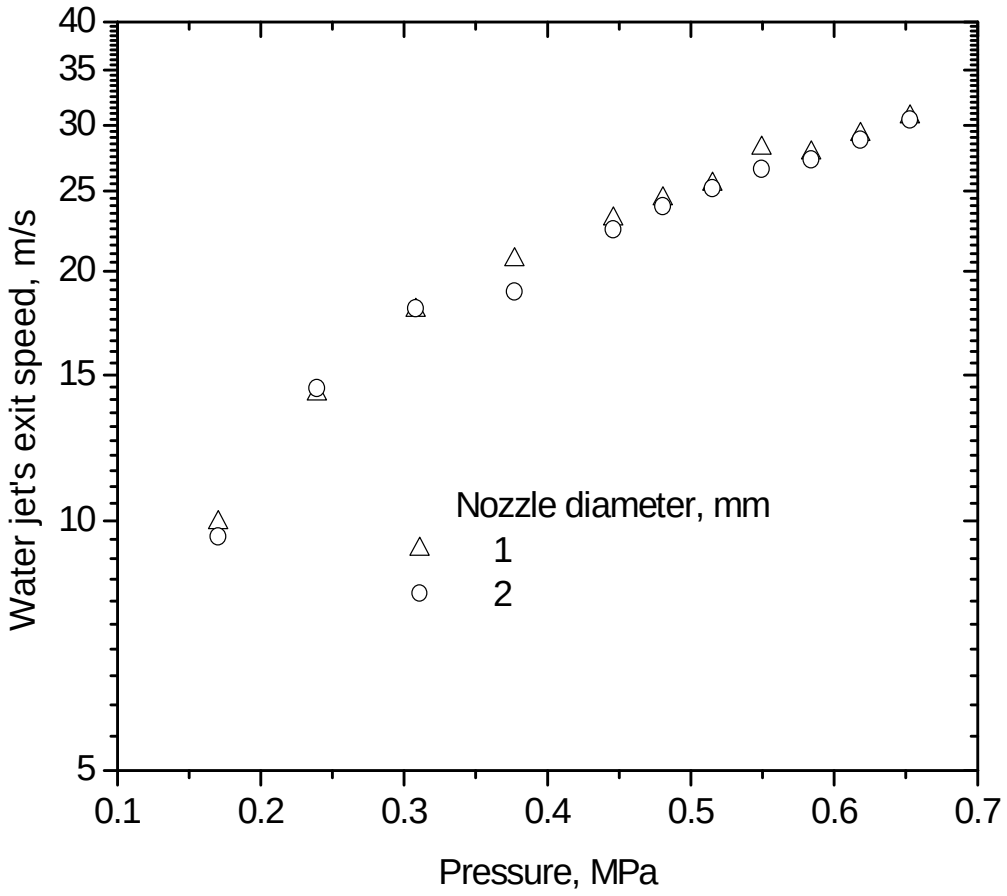

Figure 4.1. Speed of water jet for various injector pressures.

4.2 Airflow Characterization

A 2D (TSI) Laser Doppler velocimetry is used to characterize the cross airflow. The operating technique for the 2D LDV has been described briefly in the previous section. The speed of the fan drive to be calibrated corresponds to motor frequencies of 10, 20,

30, 40, 50, and 60 *Hz* which are controlled by an H7 True Torque, Adjustable Speed Drive. An individual run for the airflow's characterization is initialized on the Flowsizer software. This software interfaces with events happening in the test section. The PMT voltage, burst frequency, band pass filter, signal-noise-ratio, and downmix frequency are adjusted iteratively, until a very high data rate with an acceptable signal-to-noise ratio is achieved. When achieved, the measurement of the crossflow velocity and turbulence data starts. Twenty five thousand (25,000) data samples are taken to ensure reasonable statistical averaging for both the velocity vectors and turbulent quantities. The procedure is repeated for all the drive frequencies. The current experiment considered three frequencies (10, 20, 30 *Hz*) and compared the results with those reported by Iyogun [59]. The comparison is given in Figure 4.3. Since the differences were within experimental error, mean velocity values obtained by Iyogun [59] were used in computing the remaining flow quantities. Although the Flowsizer gives many details of the flow, only the mean airflow velocity and the turbulence intensity profiles in the vertical central plane of the test section are of interest here. Figure 4.2 shows the plane used for the cross airflow's characterization and the corresponding turbulence intensities.

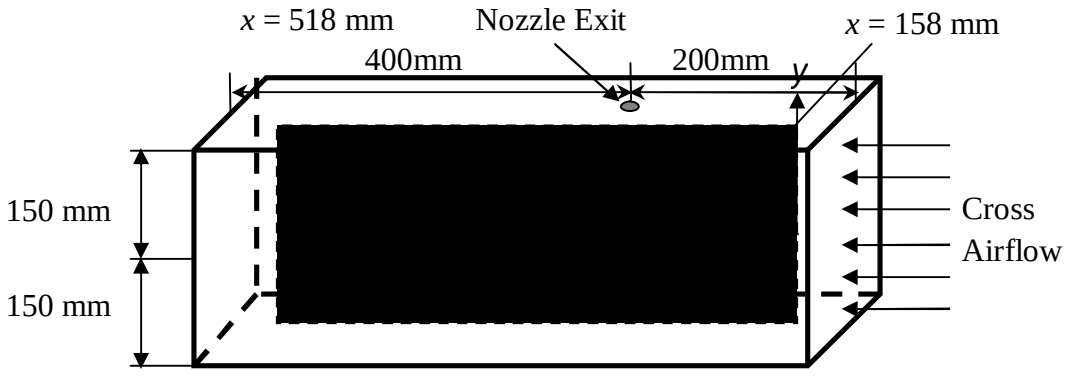

Figure 4.2. Plane for the crossflows characterization.

LDV measurements were not performed along the entire, approximately 600 *mm* length of the test section but only in the region extending from (*x* equal) 158 *mm* to 518 *mm* starting from the test section's inlet. This region and the corresponding *x* and *y* co-ordinates, which are illustrated in Figure 4.2, is sufficiently large to ensure there is a well controlled airflow in the area of the jet. The distance between neighbouring measurement stations at the center of the test section is 40 *mm* for the 10 Hz to30 *Hz* drive frequencies. The distance from the walls of the test section during measurements is 1 *mm* and this spacing is increased to 2 *mm* after a downstream distance of 20 *mm*. The distance between the data measurement points is increased to 40 *mm* around the center of the test section. Velocity measurements along the two central orthogonal planes are entirely symmetrical so that only the velocity profiles along the central vertical plane are presented explicitly. Figures 4.4 through 4.6 give the airstream's typical mean velocity distribution near the injector nozzle's location and along the entire vertical central plane. Only the data measured at 20 and 30 *Hz* are presented. Figures 4.7 through 4.9 display the corresponding turbulence intensity profiles.

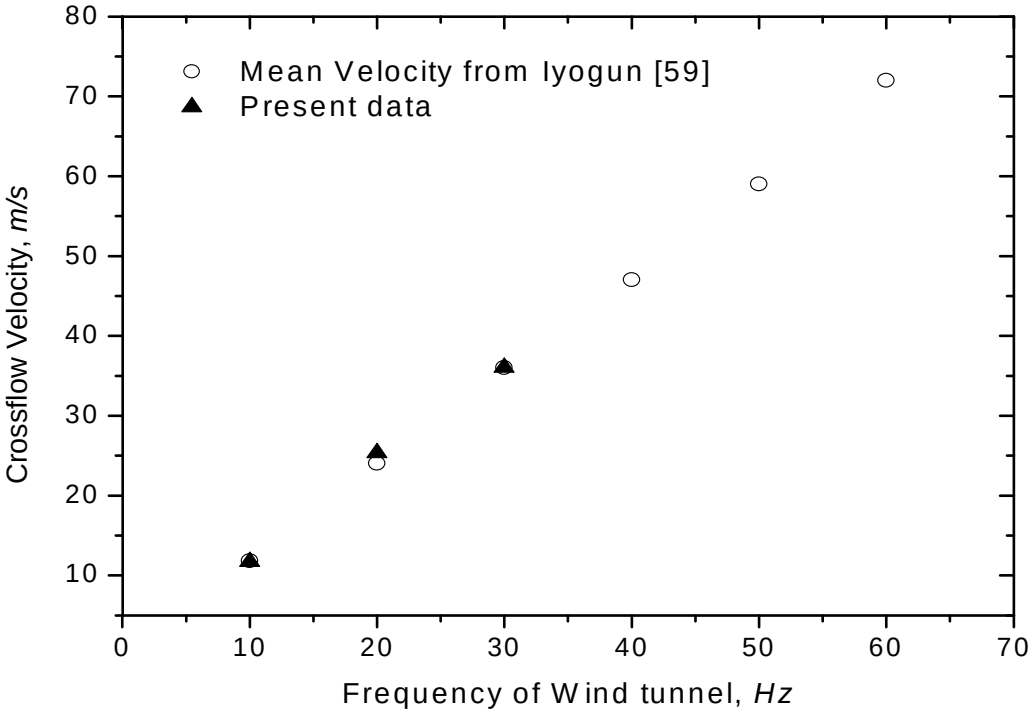

Figure 4.3. Comparison with data of Iyogun [59].

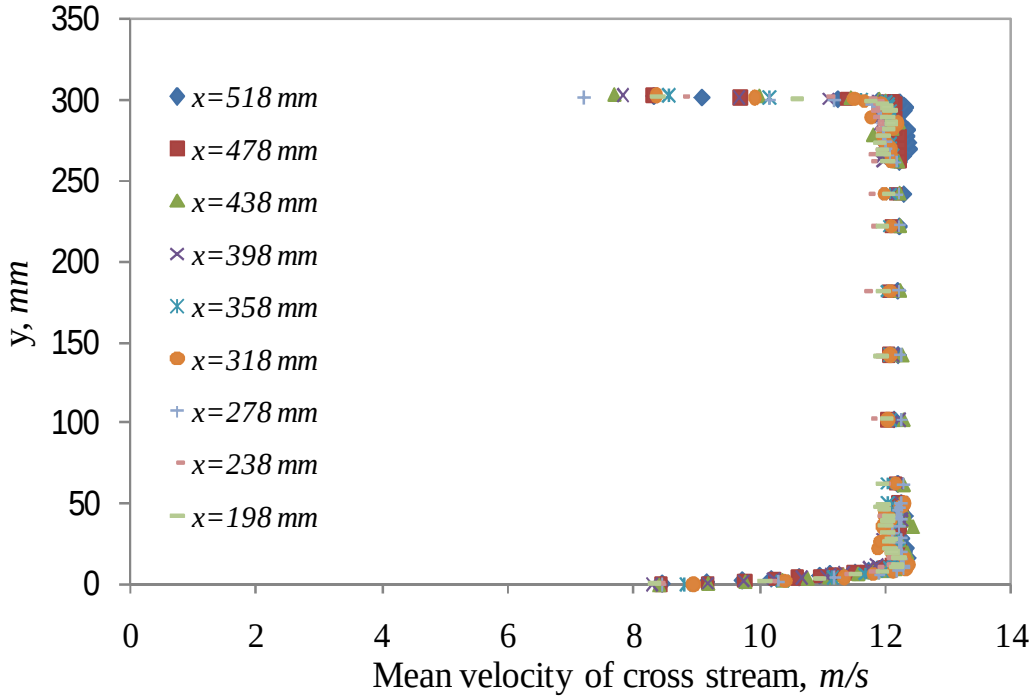

Figure 4.4. Mean velocity profile for a crossflow speed of 11 *m/s*.

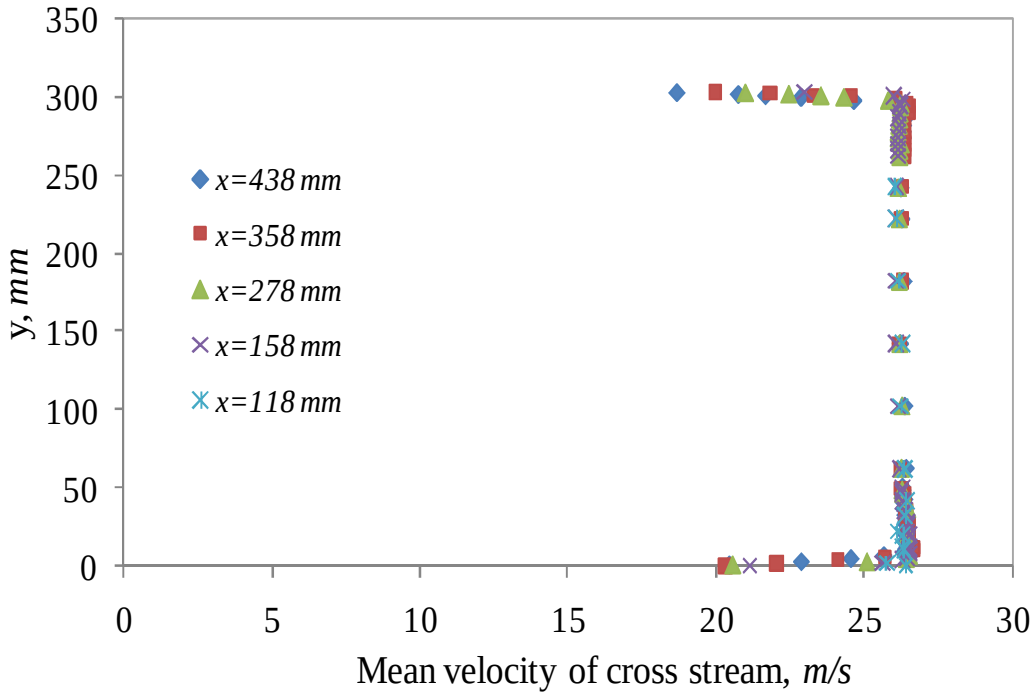

Figure 4.5. Mean velocity profile for a crossflow speed of 25*m/s*.

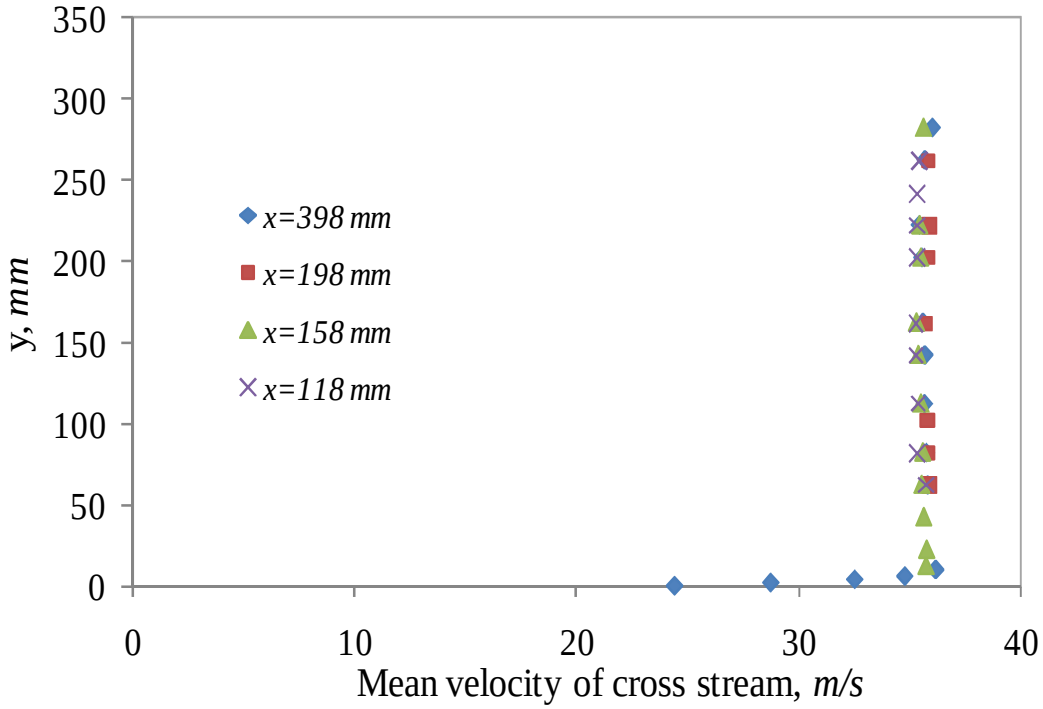

Figure 4.6. Mean velocity profile for a crossflow speed of 36 *m/s*.

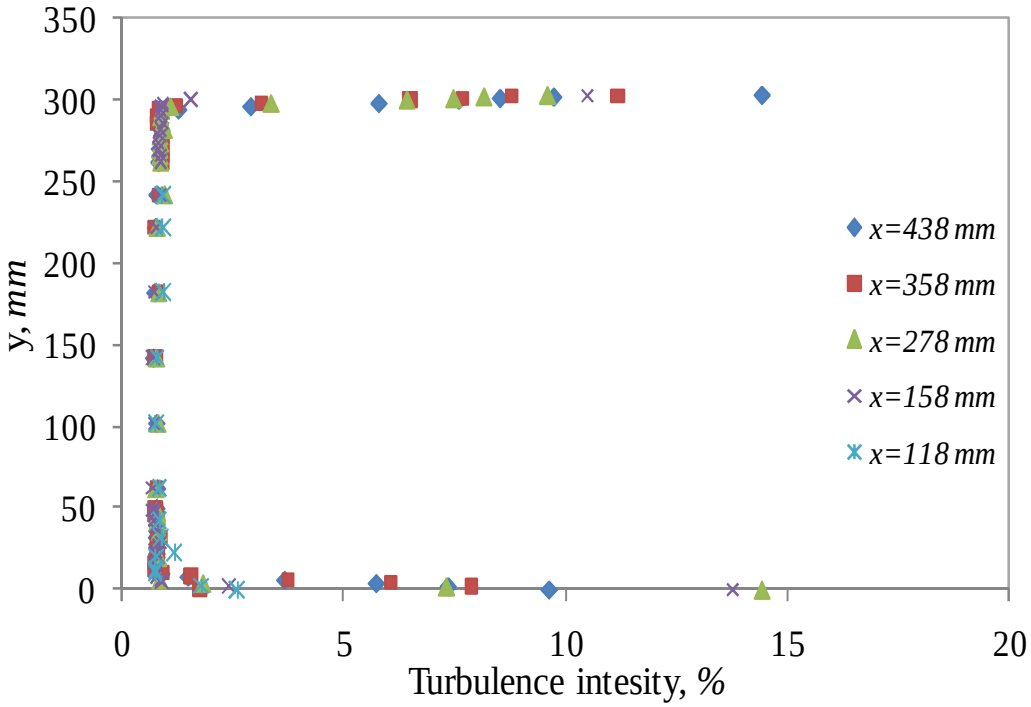

Figure 4.7. Turbulence intensity for a crossflow speed of 25*m/s*.

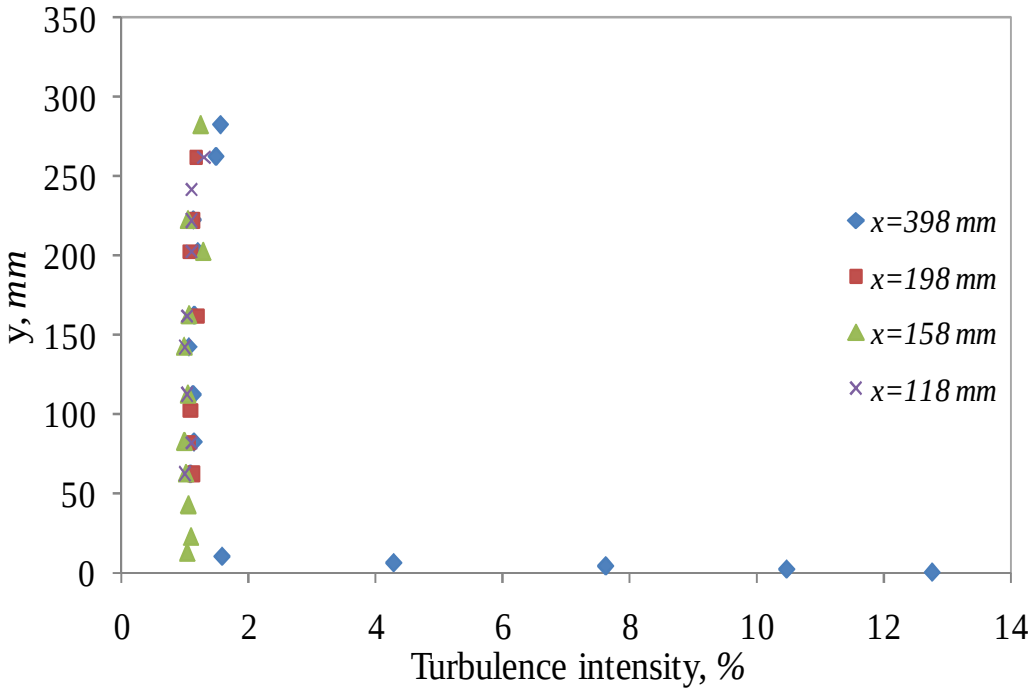

Figure 4.8. Turbulence intensity for a crossflow speed of 36 *m/s*.

The previous figures indicate clearly that, for each of the drive frequencies used, the mean velocity profiles overlapped regardless of the measurement plane considered. This consistency demonstrates that the airflow distribution is reasonably uniform throughout all the test section except for the thin boundary layer near the section's wall.

Figures 4.4(a) through (c) show that, except in the boundary layer, the turbulence intensity is about 1% even for the highest fan-speed. The boundary layer thickness is found to increase with airflow speed but it remains a relatively small 7.5 *mm* for the higher speeds of 47 and 71 *m/s* and 5 *mm* for speeds between 12 and 36 *m/s*.

Chapter 5

RESULTS AND DISCUSSION

5.1. Water Jet in Quiescent Atmosphere

5.1.1. Visualization of the jet's near-field

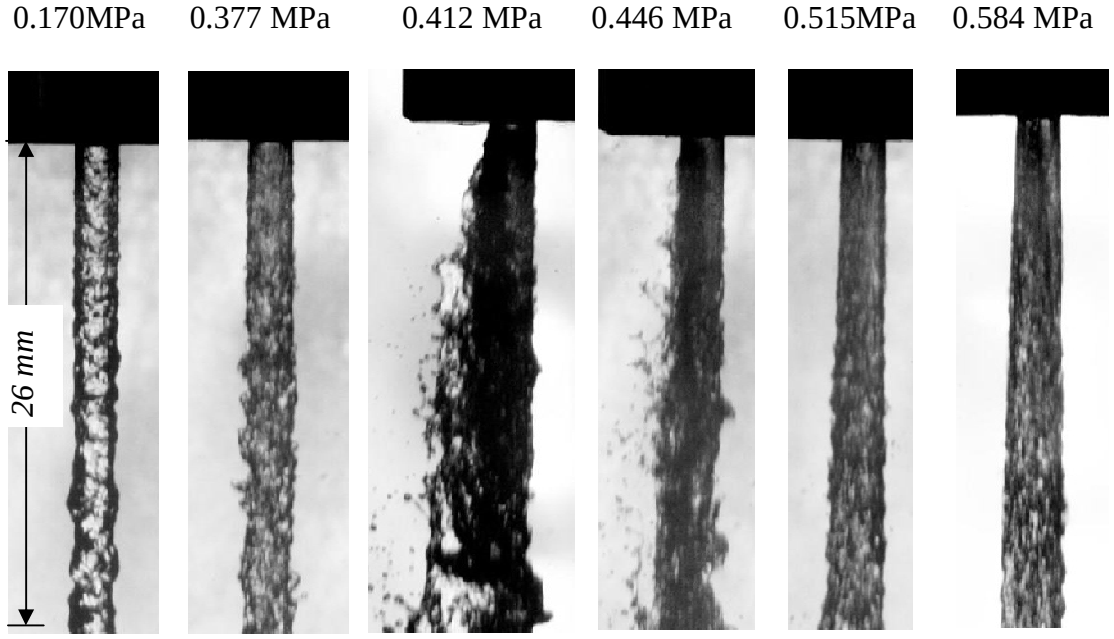

Figure 5.1. Jet issuing from Nozzle N5 into quiescent atmosphere at different water injection pressures.

The jet near field was imaged to examine the conditions under which cavitation and hydraulic flip would occur. Figure 5.1 shows how the resulting shape of a water jet from the N5 nozzle changes as the injection pressure is increased. It can be seen that the water jet has a smooth appearance at the two lowest injection pressures. On the other hand, the water jet is atomized at the two intermediate pressures of 0.412 to 0.446 *MPa*. A further increase in pressure to 0.515 *MPa* caused the spread of cavitation bubbles downstream from the entrance to the exit of the nozzle orifice which led to the emergence of a smooth water jet. This situation persisted when the injection pressure is increased to 0.584 *MPa*. An examination of a water jet column injected at high pressures into a quiescent

atmosphere through a transparent nozzle revealed that 1) the inception of cavitation inside the nozzle orifice causes the jet column to experience atomization, and 2) the occurrence of hydraulic flip leads to a smoother jet column [12, 13, 29]. Cavitation occurs when air bubbles are trapped within the liquid jet as the local pressure falls below the vapour pressure [18], and hydraulic flip occurs when the liquid jet detach from the internal surface of the nozzle [18]. Therefore, based on the water jet images shown in Figure 2, the water jet experience atomization at injection pressures of 0.412 *MPa* and 0.446 *MPa* which is believed to be caused by the inception of cavitation (and the smooth water jet at higher injection pressures (0.515 *MPa* and 0.584 *MPa*) is an indication that the jet is experiencing hydraulic flip (Ahn et al. [29], and Tamaki et al. [12, 13]). The cavitation bubbles rendered the water jet turbulent, and as it approaches the nozzle exit, the water jets becomes more turbulent and unsteady [29]. Plots of turbulent intensity profiles of the water jet in the near-field have been presented in Appendix C. The water jet's atomization under turbulent regimes is attributed to the radial velocity component which causes a disruption of the jet surface film [62].Additional images of water jet in quiescent atmosphere have been presented in Appendix C. The transition process between cavitation and hydraulic flip has been detailed by Soteriou et al. [63].

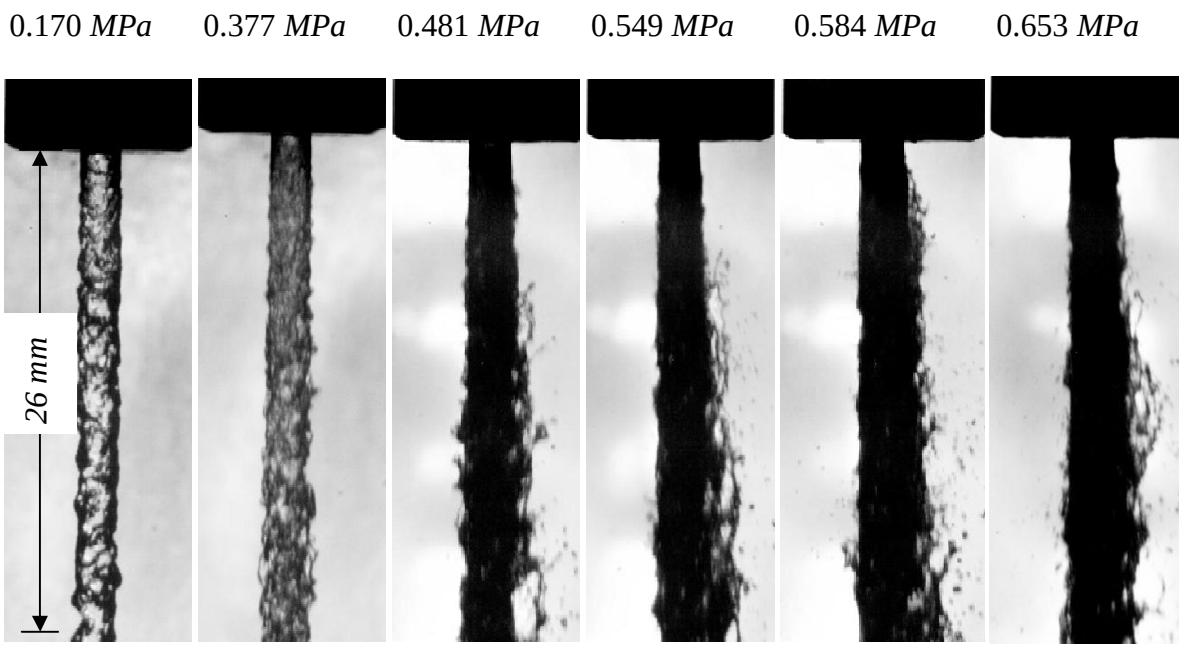

Figure 5.2. Jet issuing from Nozzle N7 into quiescent atmosphere at different water injection pressures.

5.1.2. Jet Breakup Length

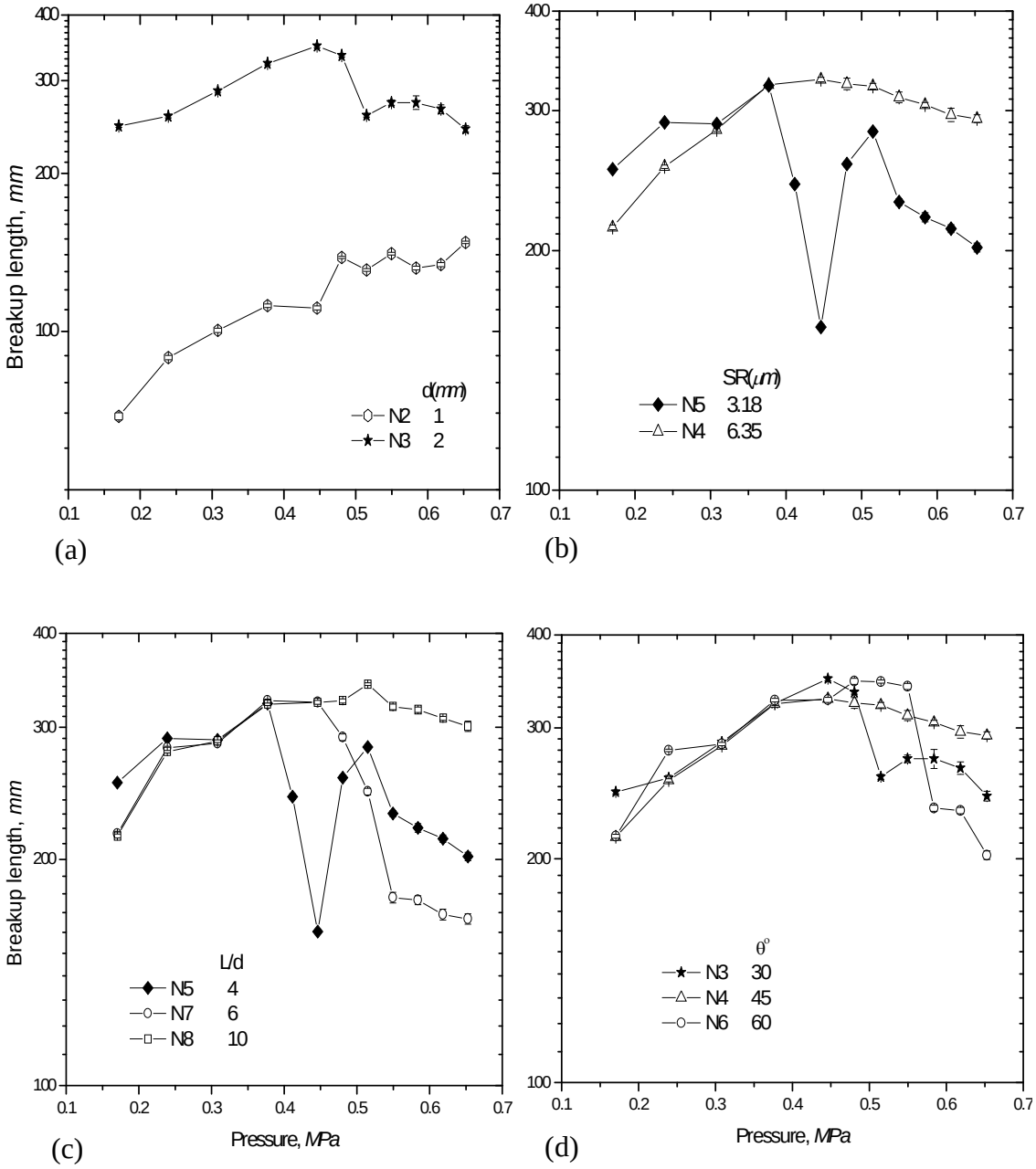

Figure 5.3. Water jet's breakup length in quiescent atmosphere for (a) θ=30°, L/d=4, SR=6.35μm, (b) θ=45°, L/d=4 (c) θ=45°, SR=3.18μm and (d) L/d=4, SR=6.35μm.

To verify further that the liquid jet experiences cavitation and hydraulic flip under certain conditions, breakup length of the jet column was calculated from the images using an in-house developed MATLAB code. Figure 5.3 illustrates the breakup length of water jet in quiescent atmosphere under a wide range of test conditions (nozzle geometry and injection pressure). For a typical water jet, the breakup length increases with injection pressure under non-cavitating flow conditions. As cavitation sets in, the breakup length shortens as a result of immense atomization of the water jet due to the inception and collapse of the cavitation bubbles. Eventually, when the water jet detaches from the surface of the nozzle, longer breakup lengths are measured as quantified and reported by Tamaki et al. [12, 13]. This is due to the spread of cavitation bubbles from the nozzle's entrance through to the exit. The current experimental breakup length pattern followed the trend of water jet breakup length under these three flow regimes reported by Tamaki et al. [13]. Based on the current results and published results by Tamaki et al [12, 13], as well as observations by Ahn et al. [29] and Song et al. [32], we can confidently assert that flow through the current nozzles experienced cavitation and hydraulic flip under certain test conditions. The plots in Figure 5.3 depict flow through the different injector nozzles utilized in the current experiment. Standard errors were found to be low for the water jet's breakup length at different injection pressures, as shown in Figure 5.3. The injector geometry under consideration was orifice exit diameter, nominal surface roughness, length-to-diameter ratio and injector contraction angle. The water jet's breakup length under these geometries conditions is discussed below.

5.1.2.1. Effect of Nozzle Diameter

It was seen from Figure 5.3(a) that increasing the nozzle's exit diameter generated longer water columns. The water jet's breakup length in quiescent atmosphere was dominated

by liquid turbulence and cavitation when present. When the nozzle diameter is increased from 1 *mm* to 2 *mm*, the effect of cavitation on the jet's breakup length is seen to diminish (Chang et al. [54]), which then led to longer water column breakup length. It is also seen in Figure 5.3(a) that the 1 *mm* nozzle has a shorter water jet breakup for the same test conditions. It can also be observed that the breakup length increases with injection pressure from 0.170 to 0.481 *MPa*, and then remained fairly constant afterwards (i.e., in the range between 0.481 and 0.653 *MPa*). This figure shows also that the jet's breakup length, issuing from the 2 *mm* nozzle, increases with injection pressure and then drops afterwards. This is attributed to the occurrence of cavitation within the injector nozzle.

5.1.2.2. Effect of Nominal Surface Roughness

The internal surface of the injector nozzle may influence the liquid jet flow by means of shear stress at the wall. The friction at the near wall promotes pressure drop and this could enhance liquid jet's turbulence (Birouk et al. [18]). Two nozzles with nominal surface roughness of 3.18 and 6.35 μm were used to study the pattern of the water jet's breakup length. It is observed from Figure 5.3(b) that longer water column's were generated for flow through the 3.18 μm nozzle at lower operating pressures (0.170 – 0.308 *MPa*). This is because the presence of roughness generated turbulent water jet and this resulted in shorter water column breakup length. Increasing the pressure, from 0.308 to 0.481 *MPa*, resulted in a sharp drop of the jet's breakup length for the water jet issuing from a nozzle with a roughness of 3.18 μm. Since the immense disturbance caused by the collapse of cavitation bubbles occurred within the nozzle, atomization of the water jet was enhanced and this shortens the jet's breakup length (see Figure 5.1 at pressures 0.412 and 0.446 *MPa*). As the injection pressure increased from 0.481 *MPa*, longer water

columns were generated. This was attributed to the occurrence of the hydraulic flip phenomenon as can be observed from Figure 5.1. Tamaki et al. [15] observed a dramatic increase in the breakup length of the water jet under hydraulic flip conditions. The jet breakup length of the 6.35 μm nozzle at the range of injection pressures from 0.377 to 0.653 *MPa* is seen to be longer than that of the 3.18 μm nozzle. This could be attributed to the intense turbulence caused by cavitation in the former nozzle. This also indicates the absence of hydraulic flip within the former nozzle. A possible reason for the reattachment of the liquid jet could be attributed to the rough burrs within the nozzle as reported by Chang et al. [54].

5.1.2.3. Effect of Nozzle Length-to-Diameter Ratio (L/d)

Three nozzles with L/d of 4, 6 and 10 were used to examine the effect of L/d on water jet. Figure 5.3(c) reports the breakup length of their corresponding water jet. It can seen that the water jet through nozzle with L/d of 4 increases with injection pressure from 0.170 to 0.377 *MPa*. Beyond this injection pressure up to 0.446 *MPa*, there is a clear drop in the jet breakup length. However, a further increase in the injection pressure up to 0.653 *MPa* appear to produce longer column breakup length, which could be due to the detachment of the liquid column from the internal surface of the nozzle [12, 13, 29, 32]. However, this figure clearly shows that increasing the nozzle's L/d to 6 and 10 resulted in the absence of any sign of the occurrence of hydraulic flip whereas the effect of cavitation persisted [11, 12, 13, 29, 42]. However, shorter water jet column breakup length is observed at in the range of injection pressure from 0.446 to 0.653 *MPa* when the nozzle's L/d is increased to 6. This is attributed to an intense atomization of the ensuing water jet (see Figure 5.2). Figure 5.2 shows that, for the water jet through the L/d = 6 nozzle, experienced atomization for the pressure range between 0.481 and 0.653 *MPa*. As for L/d

= 10 nozzle, the cavitation does not appear to affect significantly the jet's breakup length in the range of injection pressures considered in the current experiment. Finally, Figure 5.3(c) reveals that increasing the nozzle's L/d leads to the elimination of hydraulic flip since the water jet reattaches within the nozzle passage after separation [13, 29].

5.1.2.4. Effect of Nozzle Contraction Angle

The effect of a nozzles contraction angle on the breakup length of a liquid jet is still not well understood. Ghassemieh et al., [43, 58], Begenir et al. [7] and some other researchers worked extensively on nozzles with various contraction angles. Their focus, however, was more on the liquid jet properties (discharge, velocity, contraction coefficient, etc.). The current experiment therefore seeks to elucidate the effect of a nozzles contraction angles on water column breakup length. This was achieved by utilizing three injector nozzles with contraction angles of 30°, 45° and 60°. Figure 5.3(d) depicts a plot of the water jet's breakup length through each of the nozzles at various injection pressures. This figure demonstrates that the contraction angle plays a minor role on the jet's breakup length in the range of injection pressures between 0.170 and 0.446 *MPa*. However, the variation in the water jet's breakup length became evident when the injection pressure is increased from 0.446 up to 0.653 *MPa*. The onset of cavitation for the 30° contraction nozzle resulted in a sudden drop in the jet's breakup length at an injection pressure ranging between 0.481 and 0.653 *MPa*. A further increase in the injection pressure, from 0.446 to 0.653 *MPa*, resulted in a fairly constant breakup length for the water jet issuing from the 45° contraction angle nozzle. Increasing the contraction angle to 60° resulted in shorter column breakup lengths. This is attributed to the effect of droplet stripping from the main liquid column. Evidence of this is phenomenon is presented in Appendix C. Based on these results; it is worth mentioning that the effect of

cavitation on the water column's breakup length occurs at higher injection pressures and larger nozzle contraction angle. The results may be used as an indication that the water jet's breakup length is directly linked to its properties as it exits the nozzle. It was reported by Hiroyasu et al. [51] that the discharge coefficient of a nozzle with a contraction angle between 10° and 35° increases with injection pressure, meaning the flow separation region is small. Increasing the contraction angle to 45° produces flow jets with almost constant discharge coefficient which indicates that jet flow through such a nozzle have longer intact lengths. It was however reported that the discharge coefficient of a jet flow through a nozzle with a contraction angle between 60° and 120° decreases with injection pressure. This is attributed to the detachment of the liquid column from the internal surface of the nozzle, which is why shorter breakup lengths were observed at higher injection pressures as indicated in Figure 5.3(d). The ensuing liquid jet column is greatly disturbed by the inception and collapse of cavitation bubbles. Based on the present findings and published results, increasing the contraction angle of a nozzle would promote the occurrence of liquid jet separation within the nozzle, which consequently results in shorter breakup lengths.

5.1.2.5. Concluding Remarks

Although the present study did not employ transparent nozzles, the properties of the ensuing liquid jet (near-field shape presented in Figs. 5.1 and 5.2, and breakup length presented in Fig. 5.3) were used as an indication of the existence of cavitation and hydraulic flip. The conclusions were guided by published studies which employed transparent nozzles. The present study showed that nozzle geometry plays a vital role in the occurrence of these phenomena, as well as its impact on the liquid jet column's breakup length. In summary, it is seen that the water column's breakup length increases

with injection pressure for non-cavitation flow conditions. Relatively, shorter liquid column lengths were observed at the inception of cavitation. The collapse of cavitation bubbles within the nozzle causes greater disturbance and hence results in atomization of the liquid jet, which in turn results in shorter breakup lengths [12, 13, 29]. However, longer columns were measured under hydraulic flip conditions since the jet detached from the inner surface of the nozzle. This led to a noticeable increase in the water jet's breakup length as illustrated in Figure 5.3(b) [12, 13].

5.2. Water Jet in Subsonic Crossflow

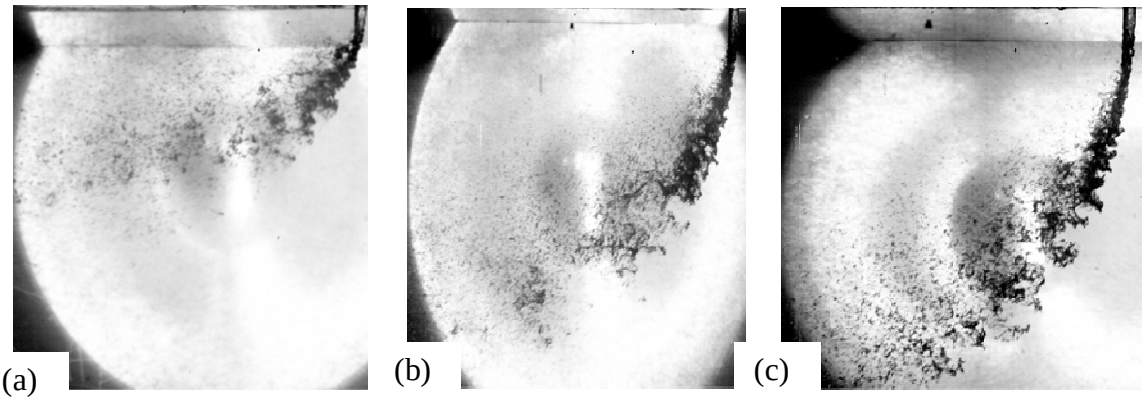

Figure 5.4. Water jet's typical penetrations at momentum flux ratios, q, of (a) 5.76, (b) 14.11, and (c) 32.01.

5.2.1. Visualization of water jet

Figure 5.4 presents images of water injected into a subsonic crossflow of air at different momentum flux ratios. The jet and crossflow injection velocities in Figures 5.4(a) through 5.4(c) are, respectively, 5.89 m/s and 70.78 m/s, 9.22 m/s and 47.02 m/s and, 9.22 m/s and 70.78 m/s. it demonstrates that a jet's penetration increases with momentum flux ratio, *q*. The trend shown in these figures agree with published observations (e.g., Iyogun et al. [37], Birouk et al. [30]). Figure 5.4 also reveals that both the liquid column's penetration and the number of drops stripped from the jet increase with *q*.

Figure 5.5 shows a comparison of the water jet's trajectory in a crossflow at typical momentum flux ratios between the present results and their published counterparts. This comparison shows clearly that the jet trajectory of the present study agrees reasonably well with published results. For instance, the jet trajectory of the present study fairly overlaps previously published results at similar q values (e.g., with Iyogun et al. [37] at q ~ 93 in Fig. 5.5(c), and Elshamy [64] at q ~ 30), and shows an increase with q values (see e.g. Fig. 5.5(b) when q varies from 4.00 to 30.91 and 14.11 to 38.56 in Fig. 5.5(a)). Figure 5.5 indicates that these findings corroborate previous observations [37, 64, 65].

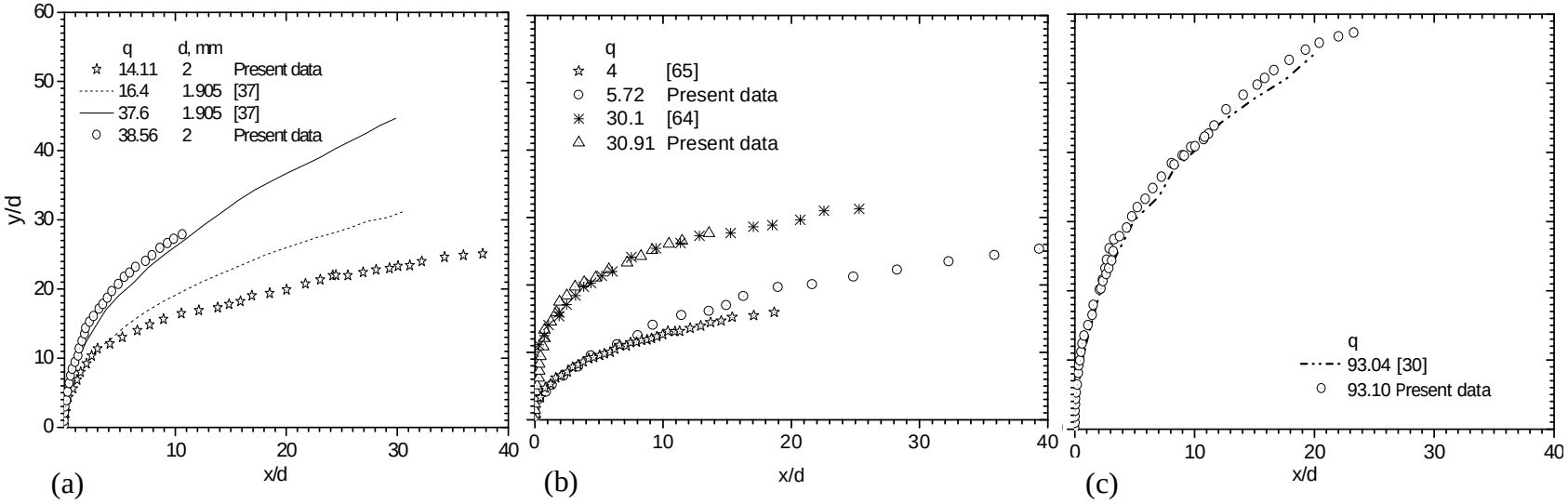

Figure 5.5. Verification of water jet's trajectory variation for different momentum flux ratios, q.

5.2.2. Jet Column's Breakup

The water jet's breakup length determined under non-cavitating, cavitation and hydraulic flip flow in subsonic crossflow are depicted in Figure 5.6. Images of the water jet taken under each of these conditions have similar breakup processes. The water column first undergoes surface breakup with growth in the acceleration waves. The water column then deforms and disintegrates into ligaments and droplets. It was reported by Schetz et al. [38] that the growth of the acceleration waves on the liquid column by aerodynamic drag forces was an important part of the breakup process. It can be recalled that for cavitation flows, the inception and collapse of cavitation bubbles cause a turbulent and unsteady water jet and this shortens the water jet's breakup length. Tamaki et al. [13] reported that the primary factor in the breakup process of a water jet was the disturbance in the flow caused by cavitation. This was achieved by measuring the vibration acceleration levels associated with the water jet's disturbance utilizing a piezoelectric acceleration transducer. With flow through the various nozzle geometries, it was observed that for lower values of q ($\leq$70), the orifice geometry played an insignificant role in the jet's breakup length. That is, under non-cavitating flow conditions, the water column breakup length increases with q in a similar manner for all nozzle geometries considered in the present study. As q increases, the effect of nozzle geometry on the jet's breakup length becomes more noticeable. This is because the water jet starts experiencing either cavitation or hydraulic flip at high values of q. In relation to the water jet's breakup length in quiescent atmosphere, the breakup length in crossflow increased with injection pressure under non-cavitating flow conditions. The rate of increase with q decreases at the inception of cavitation. Contrary to findings on longer breakup lengths under hydraulic flip conditions in quiescent atmosphere, the introduction of crossflow produced

shorter water jet column lengths. This is because when the water jet detaches from the surface of the nozzle, a smaller diameter jet exits the nozzle. The effect of the different nozzle geometries on the water column's breakup length in a subsonic crossflow is presented and discussed below.

5.2.2.1 Effect of Nozzle Diameter

Figure 5.6 illustrates the breakup length of water jet in a subsonic crossflow from different nozzle geometries. This figure reveals that the geometry of the nozzle plays a minor role in the water jet's breakup length at relatively low values of liquid/air momentum flux ratio, i.e. below approximately 70, where the liquid jet breakup length is almost the same. For example, Figure 5.6(a) shows that at values of q below 70, the two nozzles (i.e., d = 1 *mm* and d =2 *mm*) produce almost similar water jet breakup lengths where the difference is found to be within the range of experimental error. However, at momentum flux ratios greater than approximately 70, the larger diameter nozzle exhibits longer water jet column breakup lengths. At higher values of q, where cavitation occurs, ligaments are generated from the injected water jet surface and these ligaments further breakup into droplets, which led to a shorter column breakup length for the smaller orifice diameter nozzle (1 *mm*). Moreover, increasing the orifice diameter reduces the effect of cavitation on the water jet (e.g., Chang et al. [54]). Therefore longer water jet column lengths were measured for flow through the 2 *mm* diameter nozzle at higher values of q.

5.2.2.2. Effect of Length to Diameter Ratio

Three nozzles with L/d equal 4, 6 and 10 were utilized to study the jet's breakup length in subsonic crossflow. The breakup length, normalized by the nozzle's exit diameter, d, is presented in Figure 5.6(c) as a function of the momentum flux ratio, q. It clearly shows

that the jet's breakup length increases similarly for all three nozzles up to $q \sim 70$, beyond which a completely different trend is exhibited. While the jet breakup length for both nozzles with L/d = 6 and 10 continue to increase with q, but at a much slower rate than for q values below around 70, the break up length for the L/d = 4 nozzle decreases as q increases (above 70). It is interesting to remark that the nozzle with L/d = 10 produces slightly shorter breakup length than that of the L/d = 6. This is in agreement with the findings of Osta et al. [33] who reported that increasing the nozzle's L/d decreases the jet's trajectory in crossflow which is attributed to increased jet instability. Park et al. [42] attributed this difference to an increase in friction loss between the nozzle passage and liquid jet as q increases. What is more interesting in this figure is the fact that the breakup length of the water jet through the L/d = 4 nozzle drops drastically as q increases. This is due to the separation of the liquid jet from the internal surface of the nozzle orifice, which is termed as hydraulic flip phenomenon. Once the water column is separated from the surface of the nozzle (i.e., hydraulic flip), the subsonic crossflow causes waves to accelerate on the liquid column right to the nozzle exit, causing the initiation of the jet's breakup right at the nozzle exit. This consequently results in a shorter breakup length of the water jet (Ahn et al. [29]). However, as the nozzle orifice passage becomes longer, that is L/d = 6 and 10, the separated water jet reattaches to the nozzle's orifice before being discharged into the crossflow. Only cavitation occurred within these nozzles (L/d = 6, 10), which resulted in longer water jet breakup length.

5.2.2.3. Effect of Nozzle Contraction Angle

Three nozzles with contraction angles 30°, 45° and 60° were used to examine the effect of a nozzle's contraction on the jet's breakup length. Figure 5.6(d) shows, as in Figs. 5.6(a)-(c), that for q values beyond approximately 70 the increase in the jet breakup

length is at a much slower rate than for q values below about 70. More importantly, this figure shows that while nozzles with a contraction angle of 30° and 60° exhibit nearly similar breakup length, the nozzle with a contraction angle of 45° has slightly shorter breakup length. The range of nozzle's contraction angle examined in the present experiment revealed very little dependence of the jet's breakup length on the nozzle geometry.

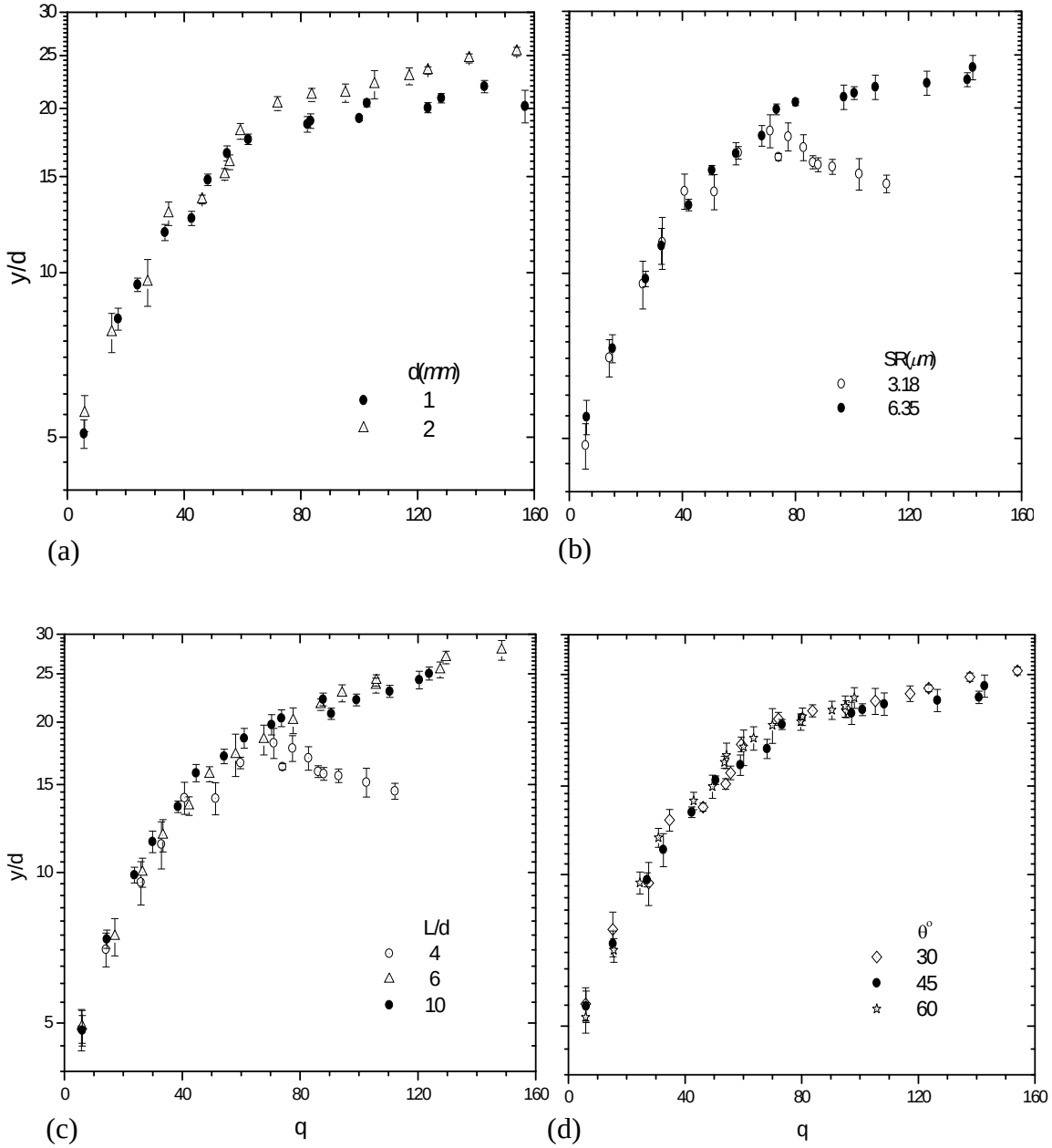

Figure 5.6. Water jet column's breakup length in subsonic crossflow for (a) θ=30°, L/d=4, SR=6.35 μm, (b) θ=45°, L/d=4, (c) θ=45°, SR=3.18 μm and (d) L/d=4, SR=6.35μm.

5.2.3. Liquid Column Trajectories

5.2.3.1 Non-cavitating Flow

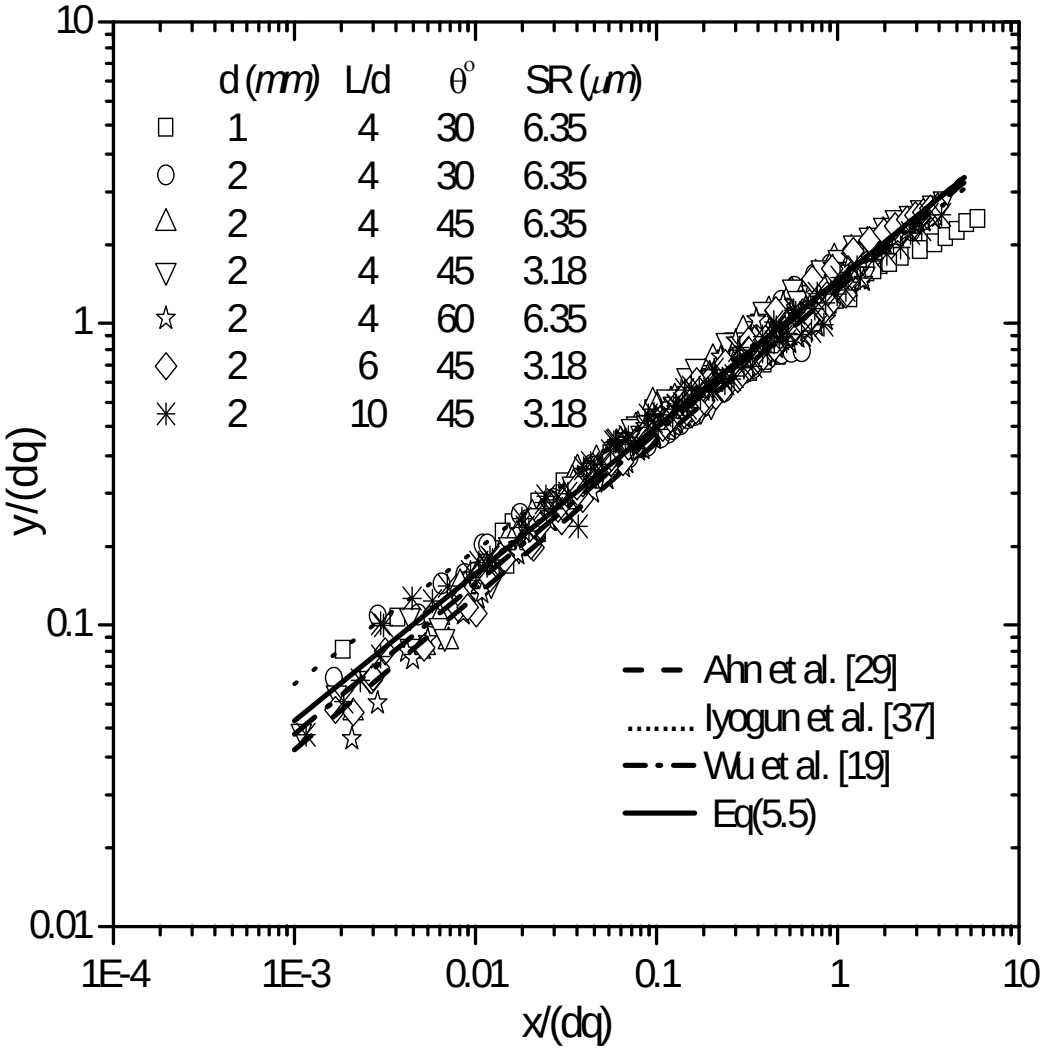

Figure 5.7. Water jet column's trajectory under non-cavitating flow conditions.

Figure 5.7 shows the present liquid jet trajectories normalized by the nozzle's exit diameter and liquid/air momentum flux ratio under non-cavitating flow for seven different nozzle geometries. The same figure presents also published results of Ahn et al. [29], Iyogun et al. [37] and Wu et al. [19] with their data correlations shown in Table 5.1 (i.e., equations (1) – (3), respectively). The comparison shown in Figure 5.7 reveals that the overall trend reasonably agrees with published correlations. The present data for non-

cavitation flow conditions for a range of q extending between 5.7 and 54 resulted in a correlation of the form as expressed in Eq. (5.5) of Table 5.1. The present correlation for the different orifice geometries is comparable to published results. Equation (5.5) is able to predict measured data with an accuracy of between ±4% to 10%, with a maximum scatter of about 15%. The correlation coefficient of a conventional regression analysis of the entire test data was 0.98 with a standard deviation less than 6%. A detailed error analysis is presented in Appendix B.

Table 5.1. Correlations describing non-cavitating water jet trajectories in a subsonic crossflow.

Reference	**Correlation ($^{y}/_{dq}$)**	**q range**	**Equation #**
Ahn et al. [29]	$1.297\left(^{x}/_{dq}\right)^{0.509}$	Not specified	(5.1)
Iyogun et al. [37]	$1.997\left(^{x}/_{d}\right)^{0.444} q^{-0.556}$	8.30 – 724	(5.2)
Wu et al. [19]	$1.370\left(^{x}/_{dq}\right)^{0.5}$	3.38 – 148	(5.3)
Song et al. [32]	$0.825\left(^{x}/_{dq}\right)^{0.5}$	Not specified	(5.4)
Present data	$1.353\left(^{x}/_{dq}\right)^{0.484}$	5.76 – 54.0	(5.5)

Figure 5.8 summarizes a water jet's trajectory from nozzles with various L/d values of 4, 6 and 10, and contraction angles, θ, of 30°, 45° and 60° under non-cavitating flow conditions. The figure suggests that the geometry of the nozzle played an insignificant role in the water jet's trajectory. The measured water jet trajectory was reasonably predicted by Equation (5.5) given that small differences are invariably within experimental errors. When the nozzle's contraction angle was increased from 30° to 60°,

there was a slight decrease in the water jet's trajectory. The difference however is within experimental errors for the contraction angles considered here. For non-cavitating flow, the water jet's trajectory was not influenced by the nozzle's geometry.

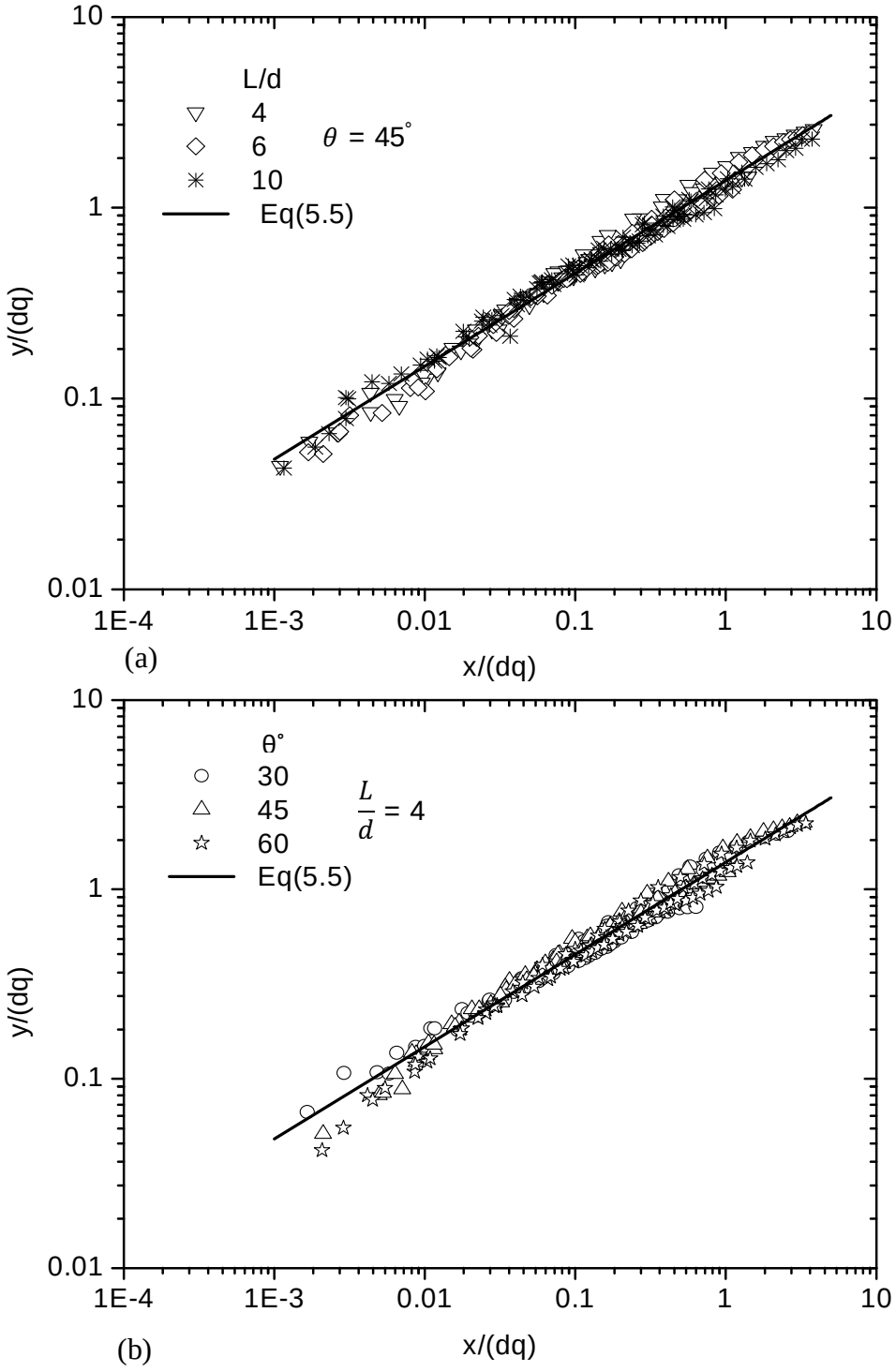

Figure 5.8. Effect of nozzle's geometry on trajectory of water jet under non-cavitating flow conditions. The internal nozzle's surface roughness is (a) 3.18 μm, and (b) 6.35 μm.

5.2.3.2. Cavitation Flow

A water jet's trajectory for a cavitating flow is compared in Figure 5.9 with the data reported by Ahn et al. [29]. For both nozzle configurations (in Fig. 5.9), a shorter trajectory data of the liquid jet was presented by Ahn et al. [29]. This is attributed partly to the non-similar nozzle configuration used in our experiment compared to theirs. However, a similar trend was acquired with all the different nozzle geometries. The present data is obtained by varying L/d and the contraction angle θ. Figure 5.9 indicate that the geometry of a nozzle has apparent small but noticeable effect on a water jet's trajectory for cavitating flows. Indeed a jet's trajectory shortens slightly as either L/d or θ increases. These trends arise from air bubbles being trapped within the jet. The cavitation causes a more turbulent jet which, in turn, increases the jet's turbulent kinetic energy. However turbulent eddies dissipate in the form of ligaments against the upcoming cross airflow so that water droplets are formed on the jet's upwind surface (Osta et al. [33]). Consequently shorter breakup lengths occur for larger L/d ratios because a jet is more unstable. Tamaki et al. [13] employed transparent nozzles, with L/d = 4 and 20, to study the effect of a nozzle internal flow on the breakup processes of a liquid jet in quiescent atmosphere. They reported that atomization of the liquid jet depends strongly on the disturbance of the liquid flow caused by the collapse of cavitation bubbles. The disturbance caused by the collapse of these bubbles is short lived when L/d = 4 but it increases when L/d is enlarged to 20 [13]. They also demonstrated that a larger L/d enhances the vibration acceleration of the jet due to the collapse of cavitation bubble. According to Tamaki et al. [13], this trend arises because the disturbance due to cavitation does not occur in the nozzle hole when L/d = 4 since only the surface of the liquid flow reattaches partially to the inner wall of the nozzle's orifice before being

discharged. In the case of L/d = 20, higher levels of vibration acceleration happen at the inception of cavitation because of the nozzle's longer passage length. Therefore, the disturbance caused by the collapsing of cavitation bubbles remain in the water jet as it travels along the surface of the nozzle. The previous explanation clarifies why there are slight variations between the water jet's trajectories presented in Figure 5.9(a). A similar trend is observed in Figure 5.9(b) when the nozzle's contraction angle was varied from 30° to 60°. It can be recalled that, in a quiescent atmosphere, increasing a nozzles contraction angle promotes a jet's separation within the contraction which leads to a substantial cavitation.

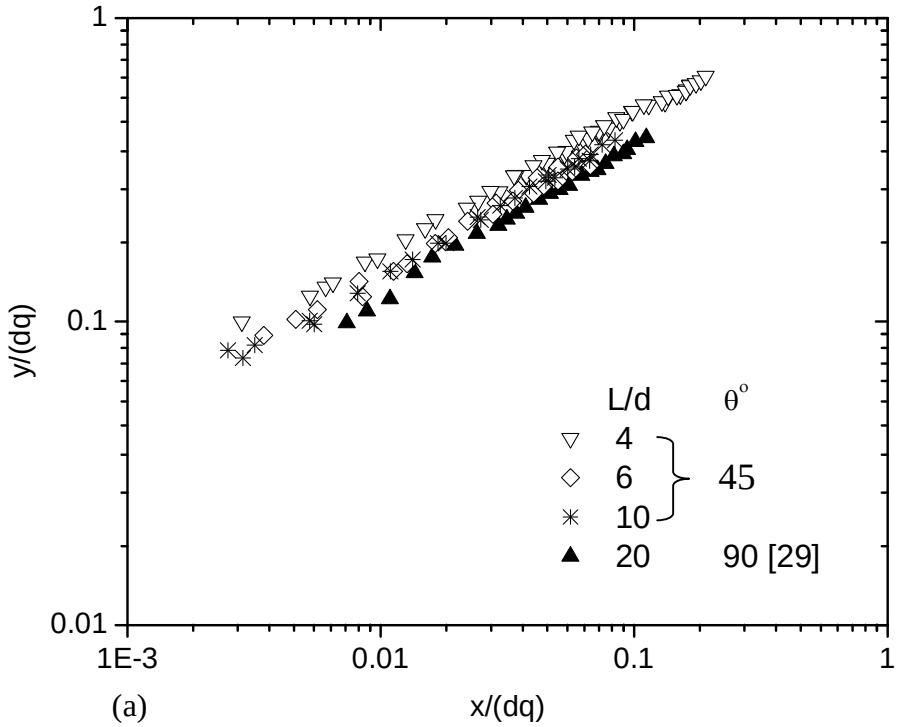

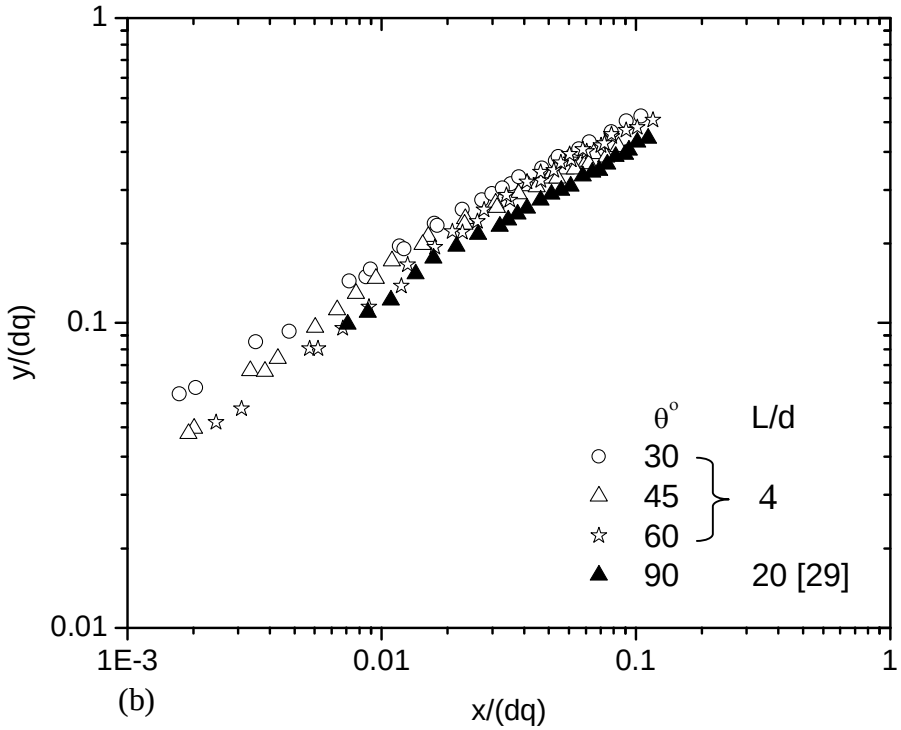

Figure 5.9. Water jet's trajectory through nozzles having various (a) L/d, SR= 3.18 μm, and (b) contraction angles, θ°, SR=6.35 μm, under cavitation flow conditions.

5.2.3.3. Hydraulic Flip Flow

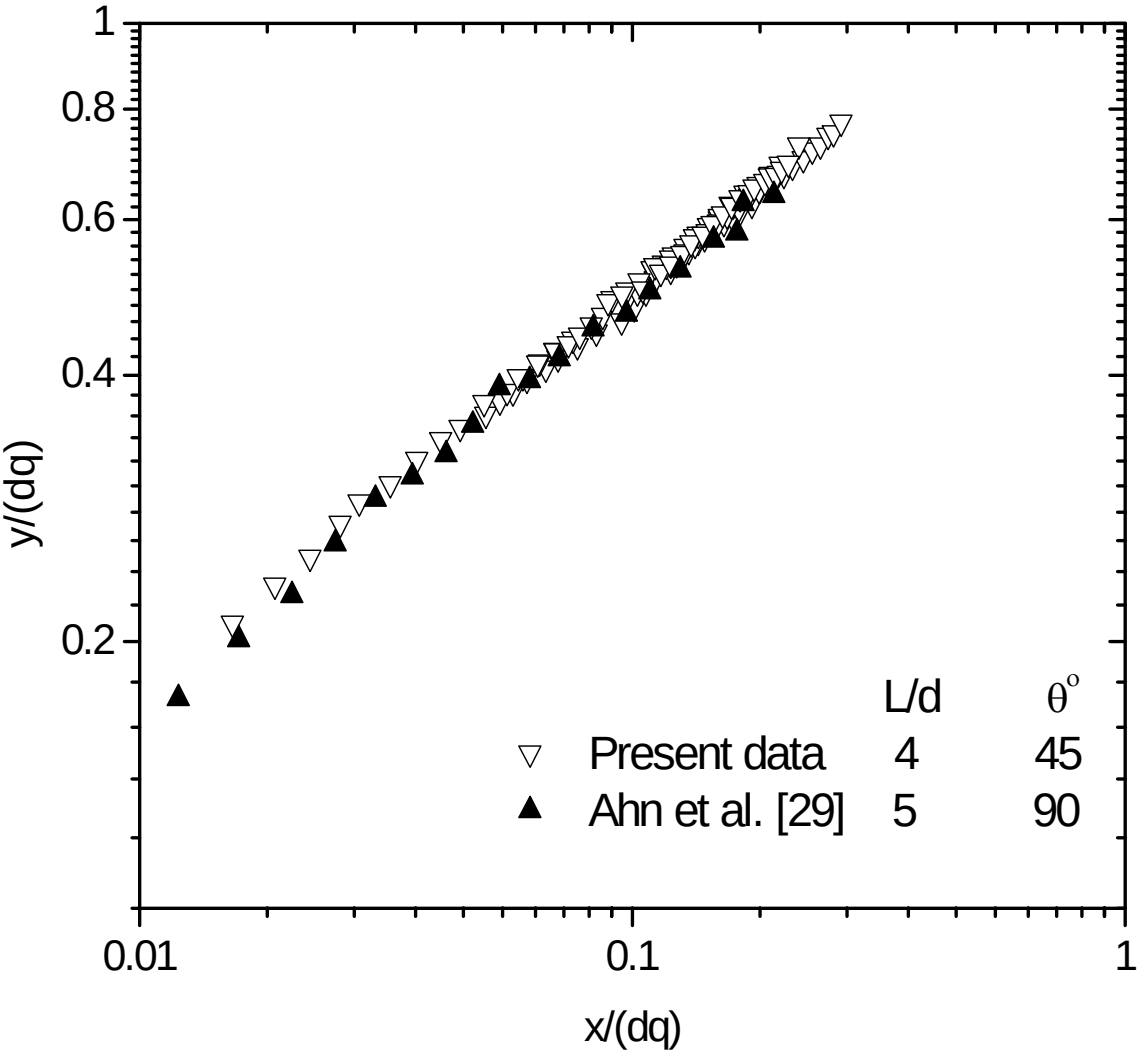

Figure 5.10. Water jet's trajectory under hydraulic flip conditions.

At the inception of hydraulic flip, a water jet detaches from the nozzle's orifice so that it produces jet having a diameter which is smaller than the nozzle's true exit diameter. Unlike cavitating flows, effective nozzle diameters and exit speeds (i.e. the momentum flux ratio) are needed to normalize the trajectory of a jet experiencing hydraulic flip. This approach has been tested by both Ahn et al. [29] and Song et al. [32]. However, their approach could not be replicated in the present study because opaque nozzles were utilized. Nonetheless, in the present study, the conventional definition of q is used in the

water jet's trajectory under hydraulic flip. Figure 5.10 compares the present water jet's trajectory with published results under hydraulic flip conditions by Ahn et al. [29]. It shows a reasonable agreement between the present data and the published results. It is clear from Figure 5.6(b) that hydraulic flip produces lower trajectories than cavitating and non-cavitating water jets. Due to the separation of the water jet experiencing hydraulic flip, where acceleration waves occur or grow on the water column and spread upstream of the nozzle's exit which ultimately cause the initiation of breakup at the nozzle's exit [29]. This agreement is attributed partly to the closeness of the L/d values used in both experiments (L/d = 4 in the present experiment and L/d = 5 in Ahn et al. [29]). Aside from the slightly dissimilar L/d ratio of the two nozzles, the small discrepancy may be attributed to the difference in the contraction angle of the two nozzles. While the present authors employed a nozzle with 45°, Ahn et al. [29] utilized a sharp edged nozzle (90°). According to Ghassemieh et al. [43, 58], sharp-edged cone-capillary nozzles having contraction angles greater than or equal to 60° yield lower discharge coefficients which is possibly due to the occurrence of hydraulic flip. The higher is the hydraulic flip the lower is the trajectory of the water jet. Therefore, the lower discharge coefficients associated with hydraulic flip and a nozzle's contraction angle could result in a lower trajectory of the water jet in subsonic crossflow.

Chapter 6

CONCLUSIONS AND RECOMMENDATIONS

6.1 Conclusions

The present thesis reported on the effects of nozzle geometry on a water jet column's breakup length and trajectories transversely injected into a subsonic crossflow. The main concluding remarks can be summarized as follows.

In quiescent atmosphere, increasing the nozzle diameter resulted in an increase in the breakup length of the water jet. The water jet's breakup length under non-cavitating flow was controlled by turbulence of the jet. This changed upon the inception of cavitation, which affected noticeably the water jet column's breakup length. Higher nominal surface roughness generated shorter water column breakup length under non-cavitating flows, and also resulted only in the occurrence of cavitation. It was observed that longer nozzle L/d resulted shorter liquid column breakup length until the onset of cavitation. Under cavitating flow conditions, increasing the nozzles L/d eliminated the occurrence of hydraulic flip phenomenon. Increasing the nozzles contraction angle promoted water jet separation within the injector nozzle. This led to shorter water jet breakup lengths. It was observed that shorter water column breakup lengths were measured under cavitating flow conditions compared to flow experiencing hydraulic flip. It was observed in subsonic crossflow that the injector nozzle geometry had an insignificant effect on the water column's breakup length at lower values of q. The differentiation in the liquid column's breakup length was made evident at higher values of q. In contrast to the breakup length in quiescent atmosphere, lower water jet columns were observed in subsonic crossflow under hydraulic flip conditions compared to cavitating flows. For non-cavitating flows,

longer water jet trajectories were measured, and the correlation obtained through seven injector nozzles were comparable to published correlations. However, compared to non-cavitating jest, lower water jet column trajectories were measured at the inception of cavitation. Moreover, jets experiencing hydraulic have shorter water jet column trajectories compared to jets experiencing cavitation.

6.2 Recommendations

- In order to predict the occurrences of both cavitation and hydraulic flip, the present study adopted the near-field images and breakup length of the water jet in quiescent atmosphere. Although practical nozzles are not made from acrylic materials, they can be used to study the internal flow of the water jet. Therefore, in order to clearly confirm the occurrence of cavitation and hydraulic flip within the non transparent nozzles, additional complementary experiments using transparent acrylic nozzles under identical test conditions are needed.
- A number of liquid jet trajectory correlations accounted for factors like temperature [68], crossflow Weber number [69] and liquid jet's viscosity [30]. This brought up the important properties that play major roles in the disintegration processes of the liquid jet. Another important nozzle characteristic (discharge coefficient) has not been thoroughly studied in crossflow to determine its effect on the liquid column's trajectory. Therefore, the pressure drop across the contraction section of the injector nozzles should be measured in future experiments. This would allow computing the discharge coefficient for flow through the various nozzles.

- Series of studies have been conducted on the liquid jet's breakup modes in subsonic crossflow [16, 21]. Various breakup modes have been reported for turbulent liquid jets [19, 21]. Ahn et al. [29] observed that the liquid jet, under non-cavitating and hydraulic flip flows, underwent surface breakup and then subsequently degenerate into droplets. The experiment however, did not look into the various breakup modes for a jet experiencing cavitation and hydraulic flip. Therefore, subsequent experiments for cavitating flows should consider the effect of cavitation on the breakup mechanisms of the liquid jet in subsonic crossflow.
- Injector nozzle diameters of 120 and 170 μm, and 127 μm were used by Ghassemieh et al. [43, 58], and Vahedi Tafreshi et al. [46] respectively in an experiment. Therefore since most practical nozzles have very small diameters, subsequent experiments should employ nozzles with diameters less than 1 mm. This would extend the practical use of the results.
- There has been conflicting reports on the effect of viscosity on the liquid jet's trajectory. Birouk et al. [30] noticed an insignificant effect of viscosity on the jet's trajectory. However, there was a visible difference in the liquid jet's trajectory when diesel and biodiesel were injected into crossflow [70]. Further studies therefore should be conducted using viscous fuels in conjunction with nozzle geometry.
- Though the nozzles contraction angle was considered in the current experiment, the range (30˚, 45˚ and 60˚) was too narrow to fully elucidate its effect on the jets trajectory especially for cavitating flows. Future experiments could consider a wide range of nozzle contraction angle (15˚ - 90˚).

REFERENCES

1. O. M. Elshamy, S. B. Tambe, J. Cai and S.-M. Jeng, Structure of Liquid Jets in Subsonic Crossflow at Elevated Ambient Pressures. AIAA (2006), pp. 14886-14895.
2. S. B. Tambe, S.-M. Jeng, H Mongia and G Hsiao, Liquid Jets in Subsonic Crossflow. 43rd AIAA Aerospace Sciences Meeting and Exhibit (2005), pp. 1-12.
3. H. P. Trinh and C. P. Chen, Development of Liquid jet Atomization and Breakup Models including Turbulence Effects. Atomization and Sprays, vol. 16 (2006), pp. 907-932.
4. O. M. Elshamy, S. B. Tambe, J. Cai and S.-M. Jeng, Excited Liquid Jets in Subsonic Crossflow. AIAA (2007), pp. 15974-15983.
5. J. Stenzler, J. G. Lee and D. A. Santavicca, Effect of Modulation of the Fuel Transfer Function of a Liquid Jet in a Crossflow. Eastern States Section Meeting of the Combustion Institute, (2001), pp. 404-407.
6. P.-K. Wu, K. A. Kirkendall, R. P. Fuller and A. S. Nejad, Spray Structures of Liquid Jets Atomized in Subsonic Crossflows. Journal of Propulsion and Power, vol. 14 (1998), pp. 173-182.
7. A. Begenir, H. V. Tafreshi and B. Pourdeyimi, Effect of Nozzle Geometry on Hydroentangling Water Jets: Experimental Observations. Textile Research Journal, vol. 74 (2004), no. 2, pp. 178-184.
8. V. Srinivasan, A. J. Salazar and K. Saito, Investigation of the Primary Breakup of Round Turbulent Liquid Jets using LES/VOF Technique. AIAA (2006), pp. 2089-2106.
9. P.-K. Wu, L.-P. Hsiang and G. M. Faeth, Aerodynamic Effects on Primary and Secondary Breakup. Liquid Rocket Engine Combustion Instability, ed., V. Yang and

W. Anderson, Progress in Astronautics and Aeronautics, AIAA, Washington, DC, (1995), pp. 247-279.

10. P.-K. Wu and G. M. Faeth, Aerodynamic Effects on Primary Breakup of Turbulent Liquids. Atomization and Sprays, vol. 3 (1993), pp. 265-289.
11. H. K. Suh and C. S. Lee, Effect of Cavitation in Nozzle Orifice on the Diesel Fuel Atomization Characteristics. International Journal of Heat and Fluid Flow, vol. 29 (2008), pp. 1001-1009.
12. N. Tamaki, K. Nishida, H. Hiroyasu and M. Shimizu, Effect of Internal Flow in a Nozzle Hole on the Breakup Processes of a Liquid Jet. International Journal of Fluid Mechanics Research, vol. 24 (1997), nos. 4-6, pp. 461-470.
13. N. Tamaki, M. Shimizu and H. Hiroyasu, Enhancement of the Atomization of a Liquid Jet by Cavitation in a Nozzle Hole. Atomization and Sprays, vol. 11 (2001), pp. 125-137.
14. T. H. New, T. T. Lim and S. C. Luo, Effects of Jet Velocity Profiles on a Round Jet in Cross-Flow. Experiments in Fluids, vol. 40 (2006), pp. 859-875.
15. C.-L. Ng, R. Sankarakrishnan and K. A. Sallam, Bag Breakup of Non-turbulent Liquid Jets in Crossflow. International Journal of Multiphase Flow, vol. 34 (2008), pp. 241-259.
16. K. A. Sallam and G. M. Faeth, Surface Properties During Primary Breakup of Turbulent Liquid Jets in Still Air. AIAA Journal, vol. 41 (2003), no. 8, pp. 1514-1524.

17. P.-K. Wu, K.-C. Lin, T. A. Jackson, Effects of Flow Initial Conditions on Spray Characteristics with and without Crossflows. 44th AIAA Aerospace Sciences Meeting, v 24 (2006), pp. 17979-17991.
18. M. Birouk and N. Lekic, Liquid Jet Breakup in Quiescent Atmosphere: A Review. Atomization and Sprays, vol. 19 (2009), no. 6, pp. 501-528.
19. P.-K. Wu, K. A. Kirkendall, R. P. Fuller and A. S. Nejad, Breakup Processes of Liquid Jets in Subsonic Crossflows. Journal of Propulsion and Power, vol. 13 (1997), pp. 64-73.
20. G. Vich and M. Ledoux, Investigation of a Liquid Jet in a Subsonic Cross-Flow. Proc. Int. Conf. Liquid Atomization and Sprays Systems, Seoul, Korea, (1997), pp. 23-30.
21. J. Mazallon, Z. Dai and G. M. Faeth, Primary Breakup of Nonturbulent Round Liquid Jets in Gas Crossflows. Atomization and Sprays, vol. 9 (1999), pp. 291-311.
22. A. Bellofiore, A. Cavaliere and R. Ragucci, Air Density Effect on the Atomization of Liquid Jets in Crossflow. Combustion Science and Tecnology, 179:1 (2007), pp. 319-342.
23. A. Bellofiore, P. Di Martino, A. Cavaliere and R. Ragucci, Atomization and Bending of Coherent Deformed Jets in Crossflow. Proceedings of the European Combustion Meeting (2005), pp. 1-6.
24. C. Aalburg, K. A. Sallam and G. M. Faeth, Properties of Nonturbulent Round Liquid Jets in Uniform Crossflows, AIAA Paper (2004), pp. 12074-12085.
25. T. Inamura, Trajectory of a Liquid Jet Traversing Subsonic Airstreams. Journal of Propulsion and Power, vol. 16 (2000), no. 1, pp. 155-157.

26. T. Inamura, N. Nagai, T. Hirai and H. Asano, Disintegration Phenomena of Metallized Slurry Fuel Jets in High Speed Air Stream. Proceedings of the 5th International Conference on Liquid Atomization and Spray Systems, (1991), pp. 839-846.
27. R. D. Ingebo, Effect of Combustor Inlet-Air Pressure on Fuel Jet Atomization. AIAA (1984).
28. E. J. Gutmark, I. M. Ibrahim and S. Murugappan, Circular and Non-Circular Subsonic Iets in Crossflow. Physics of Fluids 20. (2008).
29. K. Ahn, J. Kim and Y. Yoon, Effects of Orifice Internal Flow on Transverse Injection into Subsonic Crossflows: Cavitation and Hydraulic Flip. Atomization and Sprays, vol. 16 (2006), pp. 15-34.
30. M. Birouk, C. O. Iyogun and N. Popplewell, Role of Viscosity on Trajectory of Liquid Jets in a Crossflow. Atomization and Spray, vol. 17 (2007), pp. 267-287.
31. P. K. Wu, R. F. Miranda and G. M. Faeth, Effects of Initial Flow Conditions on Primary Breakup of Nonturbulent and Turbulent Round Liquid Jets, Atomization and Sprays, vol. 5 (1995), pp. 175-196.
32. J. Song, K. Ahn, M.K. Kim and Y. Yoon, The Spray Plume Characteristics of Liquid Jets in Subsonic Crossflows. 43rd AIAA/ASME/SAE/ASEE Joint Propulsion Conference (2007), pp. 3976-3983.
33. A. Osta and K. A. Sallam, The Effect of Nozzle Length to Diameter Ratio on the Surface Properties of Turbulent Liquid Jets in Gaseous Crossflow. Journal of Power and Propulsion, vol. 26 (2010), no. 5, pp. 936 – 946.

34. J. A. Schetz and A. Padhye, Penetration Breakup of Liquids in Subsonic Airstreams, AIAA J., vol. 15 (1977), no. 10, pp. 1385-1390.
35. T. H. Chen, C. R. Smith, D. G. Schommer and A. S. Nejad, Multi-zone Behaviour of Transverse Liquid Jet in High-Speed Flow. AIAA, (1993), no. 93-0453, Reston, VA.
36. E. L. Geery and M. J. Margettes, Penetration of a High Velocity Gas Stream by a Water Jet. Journal of Spacecraft and Rockets, vol. 6 (1969), no. 1, pp. 79-81.
37. C. O. Iyogun, M. Birouk and N. Popplewell, Trajectory of Water Jet Exposed to Low Subsonic Crossflow. Atomization and Sprays, vol. 16 (2006), pp. 963-979.
38. J. A. Schetz, E. A. Kush and P. B. Joshi, Wave Phenomena in Liquid Jet Breakup in a Supersonic Crossflow. AIAA Journal, vol. (18) (1980), no. 7, pp. 774-778.
39. T. Inamura, N. Nagai, T. Watanabe and N. Yatsuyanagi, Experimental Heat Transfer, Fluid Mechanics, and Thermodynamics 1993, Proceedings of the Third World Conference, (1993), HI. Edited by M.D. Kelleher, R.K. Shah, K.R. Sreenivasan, and Y. Joshi. Amsterdam: Elsevier Science Publishers B.V., pp. 1522-1529.
40. A. S. Nejad and J. A. Schetz, Effects of Viscosity and Surface Tension on a Jet Plume in Supersonic Cross flow. AIAA Journal [0001-1452] vol. 22 (1983), no. 4, pg. 458.
41. M. Birouk, T. Stabler and B. J. Azzopardi, Primary Breakup of a Viscous Liquid in a Cross Airflow. Particle and Particle Systems Characterization, vol. 20 (2003), no. 4, pp. 283-289.
42. S. H. Park, H. K. Suh and C. S. Lee, Effect of Cavitating Flow on the Flow and Fuel Atomization Characteristics of Biodiesel and Diesel Fuels. Energy and Fluids, vol. 22 (2008), pp. 605-613.

43. E. Ghassemieh1, H. K. Versteeg and M. Acar, The Effect of Nozzle Geometry on the Flow Characteristics of Small Water Jets. Journal of Mechanical Engineering Science, vol. 220 (2006), pp. 1739-1753.

44. T. H. New, T. T. Lim and S. C. Luo, Elliptic Jets in Crossflow. Journal of Fluid Mechanics, vol. 494 (2003), pp. 119-140.

45. D. S. Liscinsky, B. Tre and J. D. Holdemen, Crossflow Mixing of Non-circular Jets. 33rd ASME, AIAA, (1995), 95-0732, pp. 1-17.

46. H. VahediTafreshi and B. Poudeyhimi, The Effect of Nozzle Geometry on Water Jet Breakup at High Reynolds Number. Experiments in Fluids, vol. 35 (2003), pp. 364-371.

47. R. A. Bunnel, S. D. Heister, C. Yen and S. H. Collicott, Cavitating Injector Flow: Validation of Numerical Models and Simulations of Pressure Atomizers. Atomization and Sprays, vol. 9 (1999), pp. 445-465.

48. D. P. Schmidt, C. J. Rutland, M. L. Corradini, P. Roosen and O. Genge, Cavitation in Two-dimensional Asymmetric Nozzles. SAE Technical Paper, no. 1999-01-0518 (1999).

49. C. Xu, R. A. Bunnel and S. D. Heister, On the Influence of Internal Flow Structure on Performance of Plain-Orifice Atomizer. Atomization and Sprays, vol. 11 (2001), pp. 335-350.

50. M. Arai, H. Hiroyasu and M. Shimizu, Similarity between the Breakup Length of High Speed Liquid Jet in Atmospheric and Pressurized Conditions. Proc. ICLASS (1991), pp. 61.

51. H. Hiroyasu, M. Arai and M. Shimizu, Breakup Length of a Liquid Jet and Internal Flow in a Nozzle. ICLASS-91 (1991), pp. 123-133.
52. J. McCarthy, Review of Stability of Liquid Jets and the Influence of Nozzle Design. Chemical Engineering Journal, vol. 7 (1974), pp. 1-20.
53. H. K. Suh and C. S. Lee, Effect of Cavitation in Nozzle Orifice on the Diesel Fuel Atomization Characteristics. International Journal of Heat and Fluid Flow, vol. 29 (2008), pp. 1001-1009.
54. J.-C. Chang, S.-B. Huang and C.-M. Lin, Effects of Inlet Surface Roughness, Texture, and Nozzle Material on Cavitation. Atomization and Sprays, vol. 16 (2006), pp. 299-317.
55. G. M. Faeth, L.-P. Hsiang and P. K. Wu, Structure and Breakup Properties of Sprays. International Multiphase Flow, vol. 21 (1995), pp. 99-127.
56. L.-K. Tseng, A. A. Ruff, P. K. Wu and G. M. Faeth, Continuous and Dispersed-Phase Structure of Pressure-Atomized Sprays, Recent Advances in Spray Combustion: Spray Combustion Measurements and Model Simulation, vol. 11, ed., K. K. Kuo, Progress in Astronautics and Aeronautics, AIAA, Washington, DC, (1996), pp. 3-30.
57. L.-K. Tseng, P. K. Wu and G. M. Faeth, Dispersed-Phase Structure of Pressure-Atomized Sprays at various Gas Densities. Journal of Propulsion and Power, vol. 8(1992), no. 6, pp. 1157-1166.
58. E. Ghassemieh, H. K. Versteeg and M. Acar, Effect of Nozzle Geometry on the Flow Characteristics of Hydroentangling Jets. Textile Research Journal, vol. 73 (2003), no. 5, pp. 444-450.

59. C. O. Iyogun, Trajectory of Liquid Jets Exposed to a Low Subsonic Cross Airflow. MSc Thesis (2005).

60. R. D. Reitz and S. P. Lin, Drop and Spray Formation from a Liquid Jet. Annual Review of Fluid Mechanics, vol. 30 (1998), pp. 85-105.

61. L. J. Chelko, Penetration of Liquid Jets into a High Velocity Air Stream. NACA, RM E50F21, (1950)

62. A. H. Lefebvre, Atomization and Sprays, (1989), Chapter 2, Hemisphere, Philadelphia.

63. C. Soteriou, R. Andrews and M. Smith, Further Studies of Cavitation and Atomization in Diesel Injection, SAE Technical Paper Series (1999), pp. 1486.

64. O. M. Elshamy, Experimental Investigations of Steady and Dynamic Behaviour of Transverse Liquid Jets. Ph.D. Thesis (2006).

65. J. B. Perurena, C. O. Asma, R. Theunissen and O. Chazot, Experimental Investigation of Liquid Jet Injection into Mach 6 Hypersonic Crossflow. Experimental Fluids, vol. 46 (2009), no. 3, pp. 403-417.

66. J. P. Holman, Experimental Methods for Engineers. Seventh Edition (2001)

67. A. J. Wheeler and A. R. Ganji, Introduction to Engineering Experimentation. Second Edition (2004).

68. R. R. Lakhamraju, Liquid Jet Breakup Studies in Subsonic Airstream at Elevated Temperatures. MSc. Thesis (2005).

69. J. Stenzler, J. G. Lee, D. Santavicca and W. Lee, Penetration of Liquid Jets in a Crossflow. Atomization and Sprays, vol. 16 (2006), pp. 887-906.

70. E. Farvardin, M. Johnson, P. Gauthier and A. Dolatabadi, Comparative Study of Penetration of Biodiesel and Diesel Jets in Gaseous Crossflow. Proceedings of Combustion Institute (2011).

Appendix A

MATLAB CODE FOR THE LIQUID JET BREAKUP LENGTH AND TRAJECTORY

For Flow in Quiescent Atmosphere

```
first=0;%First image
last=199;%Last image
threshold=238;%Selected visually
Bthreshold=2E-3;%Selected visually on the jet image  to estimate the breakup length; values less than this represent noise…

Path='';race path to file location
name=[Path 'ImgA' num2str(first, '%06d') '.tif'];%File name of first image

[X, map]=imread(name);%Read the first image to determine the map; X is the image data and map is the color map.

Ave=double(X);%Use Ave as an accumulator to later compute an average image.

%Loop over all images yet to be read
for i=first+1:1:last
i
name=[Path 'ImgA' num2str(i, '%06d') '.tif'];%Current image file name
    X=imread(name);%Read the current image data
    Ave=Ave+double(X);%Add the current image to the accumulator
end
%
Ave=double(Ave)/(last-first+1);%Compute an average image.

%Plot the average image
figure;
caxis([min(min(Ave)) max(max(Ave))]);
image(Ave);
colormap(jet(256)); %Try also hsv

%Estimate the breakup length…
Figure
%Remove all data less than the threshold…
T=Ave>threshold;
image(T);
colormap([0 0 0;1 1 1]);
AC=mean(T,1);
figure
plot(AC)
BU=find(AC>Bthreshold);
```

```
BU(BU<600)=[];
BU=min(BU)
```

Flow in Subsonic Crossflow

```
% the code averages the number of images uploaded

clear
clc
closeall

%Put the first and last image numbers
first=0;
last=30;

% Put path here
Path='; Trace path to file location on computer or storage device

%Modify file name
filename='ImgA';

%Modify file name. This generates the output file in an excel format.
excelfilename='BkComp.xls';

if first==last
name=[Path filename num2str(first, '%06d') '.tif'];
   [X, map]=imread(name,'TIFF');
   Ave=X;
else
for i=first:1:last
i
name=[Path filename num2str(i, '%06d') '.tif'];
      [X, map]=imread(name);
if i~=first
         Ave=Ave+double(X);
else
         Ave=double(X);
end
end
   Ave=uint8(round(Ave/(last-first+1)));
end

figure;
image(Ave);
colormap(map);
maximize(gcf);
```

```
[x,y]=getpts;
xlswrite(excelfilename, [x y]);
```

Appendix B

UNCERTAINTY ANALYSIS

The procedure to determine the uncertainty (i.e. the bias, *B*, and precision, *P*) in the measured quantities follows that given in [66, 67]. The primary sources of the bias uncertainties arise from the camera's resolution, as well as its field of view calibration, and the errors created in the basic measurements. Precision errors are the result of a spray's unsteadiness. Both types of error are reduced by increasing the number of separately obtained samples.

The equation of a water jet's trajectory in a subsonic crossflow takes the general form:

$$\frac{y}{dq} = C\left(\frac{x}{dq}\right)^{n}. \qquad (B.1)$$

The bias error is based on the sensitivity coefficients *C* and *n* used in Equation B.1. These coefficients are treated as variables in Table B1.Theirmagnitudes, which are given in Table B1, are obtained from a linear regression analysis. To determine the corresponding bias error, Equation *(B.2)*given below is used. In general

$$B_{y/d}^2 = \eta_C^2 B_C^2 + \eta_n^2 B_n^2 \equiv \sum_{v=C,n} \eta_v B_v^2 \qquad (B.2)$$

Where η_v are the generic form of the two sensitivity coefficients which are defined as $\eta_v = \frac{\partial(y/d)}{\partial v}$. Note that subscript v is a dummy variable indicating either *C* or *n*, where applicable. The values of B_v given in Table B1 are determined from their accuracies. For example, comparing the 1.353 value of *C* from the present work to corresponding 1.370 reported by Wu et al. [19], there is a difference of 1%. Table B1 also gives illustrative bias error limits for a typical water jet from a nozzle having an internal diameter, d = 2 *mm*, q = 14.11. Measurements are taken at a streamwise location of 24.23*mm*.

Table B1.Illustrative bias errors.

Variable,v	Magnitude	B_v	η_v	$B_v\eta_v$	$B_v\eta_v/\sum B_v\eta_v$	$(B_v\eta_v)^2$
C	1.353	0.010	3.345	0.034	0.984	0.001
n	0.484	0.001	143.236	0.143	0.543	0.020

The bias, $B_{y/d}$, introduced by the measurements of the jet's normalized penetration, *y/d* is found from Equation *(B.2)* and Table B1 to be$[0.001 + 0.020]^{1/2}$ or 0.15.

The precision component, $P=\frac{t\sigma}{n}$, of the uncertainties is determined by their standard deviation as well as the mean of the data, $\left(y/d\right)_m = \frac{1}{n}\sum_{i=1}^{n}\left(y/d\right)_i$. The standard deviation which arises at a downstream location, *y/d* of 16.9, in the case of the illustrative water jet's trajectory, is rounded up conservatively to 4%. The *t* is the confidence coefficient which is 2at the 95% confidence level according to [66]. The number of samples, *n*, for the experiment is 50. Finally, the standard deviation, σ, is defined as

$$\sigma = \left[\frac{\sum_{j=1}^{n}\left((y/d)_j-(y/d)_m\right)^2}{n-1}\right]^{1/2} . \qquad (B.3)$$

where the $\left(y/d\right)_j$ $j=1, 2, 3...n$, are the individual normalized jet trajectories at a streamwise location of 24.23 *mm*. Therefore, with known values of σ, *t* and *n*, the precision error can be determined straight forwardly to be 0.002. The resulting ***total error***, ε, is given [67] by Equation *(B.4)* below, as

$$\varepsilon = (B^2 + P^2)^{1/2} \quad . \qquad (B.4)$$

Hence the calculated value of ε is $[0.15^2 + 0.002^2]^{1/2}$ or 0.15. Clearly the bias error dominates.

Appendix C

EXTRA PLOTS FOR JETS IN QUIESCENT ATMOSPHERE AND SUBSONIC CROSSFLOW

0.170 *MPa* 0.377 *MPa* 0.446 *MPa* 0.515 *MPa* 0.584 *MPa*

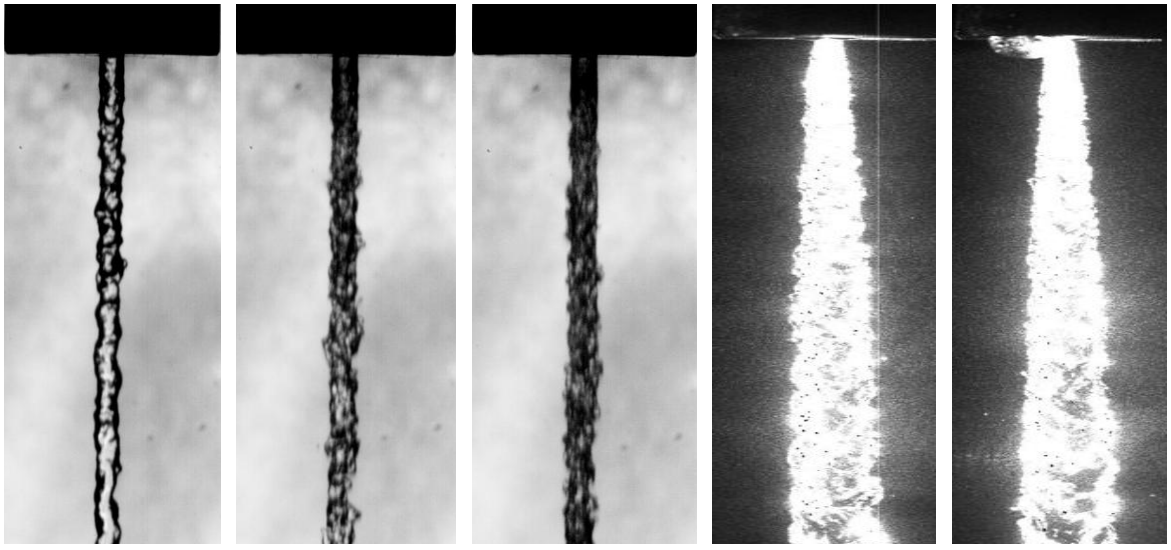

Figure C.1. Jet issuing from Nozzle N2 into quiescent atmosphere at different water injection pressures.

0.170 *MPa* 0.377 *MPa* 0.446 *MPa* 0.515 *MPa* 0.584 *MPa* 0.618 *MPa*

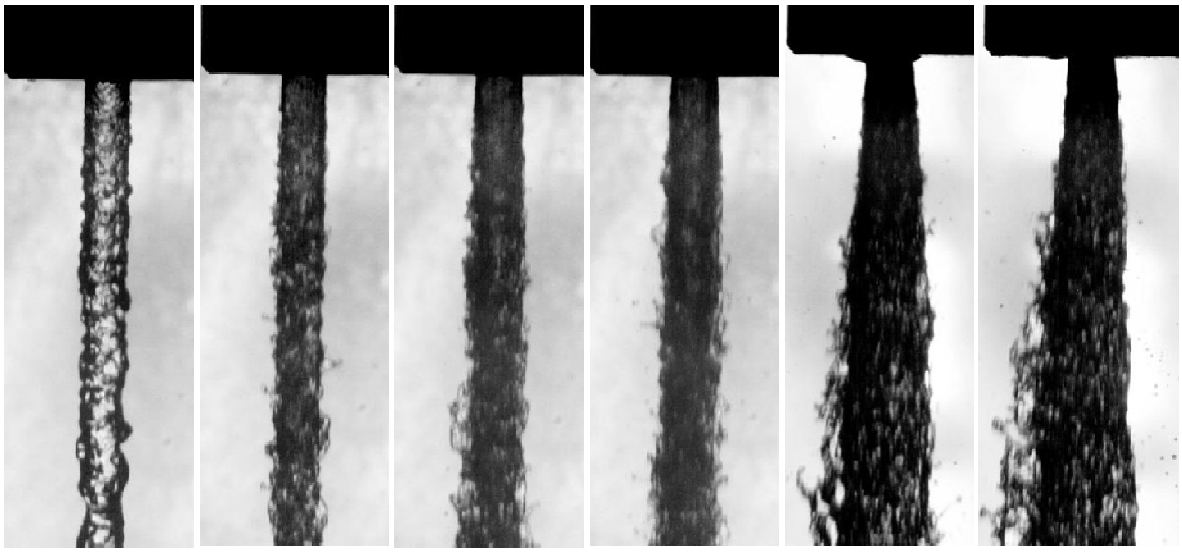

Figure C.2. Jet issuing from Nozzle N4 into quiescent atmosphere at different water injection pressures.

0.170 *MPa* 0.377 *MPa* 0.446 *MPa* 0.515 *MPa* 0.549 *MPa* 0.584 *MPa*

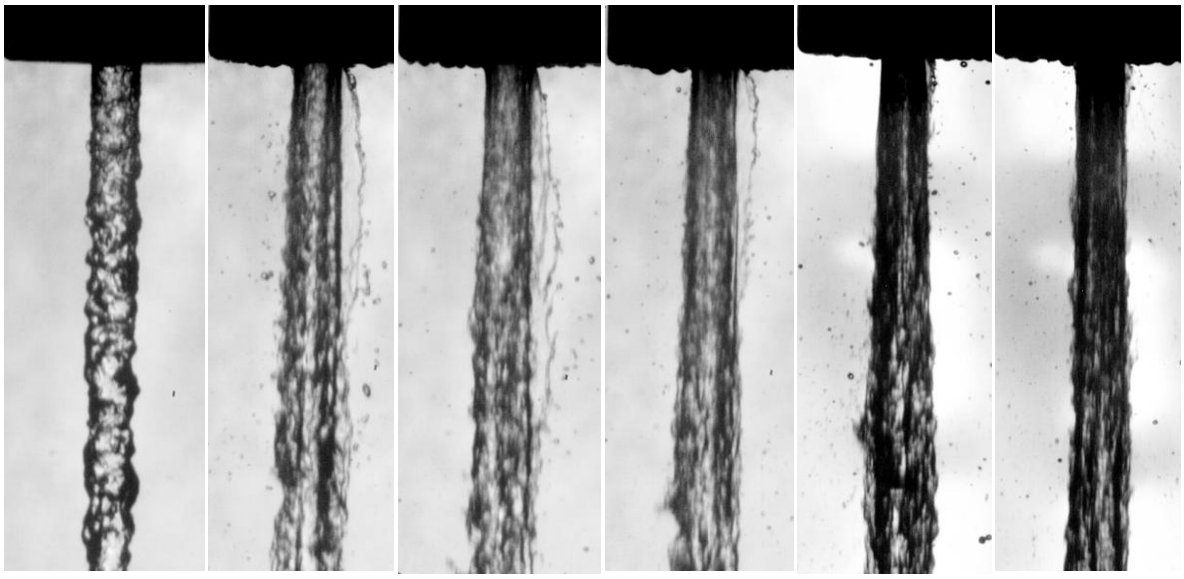

Figure C.3. Jet issuing from Nozzle N6 into quiescent atmosphere at different water injection pressures.

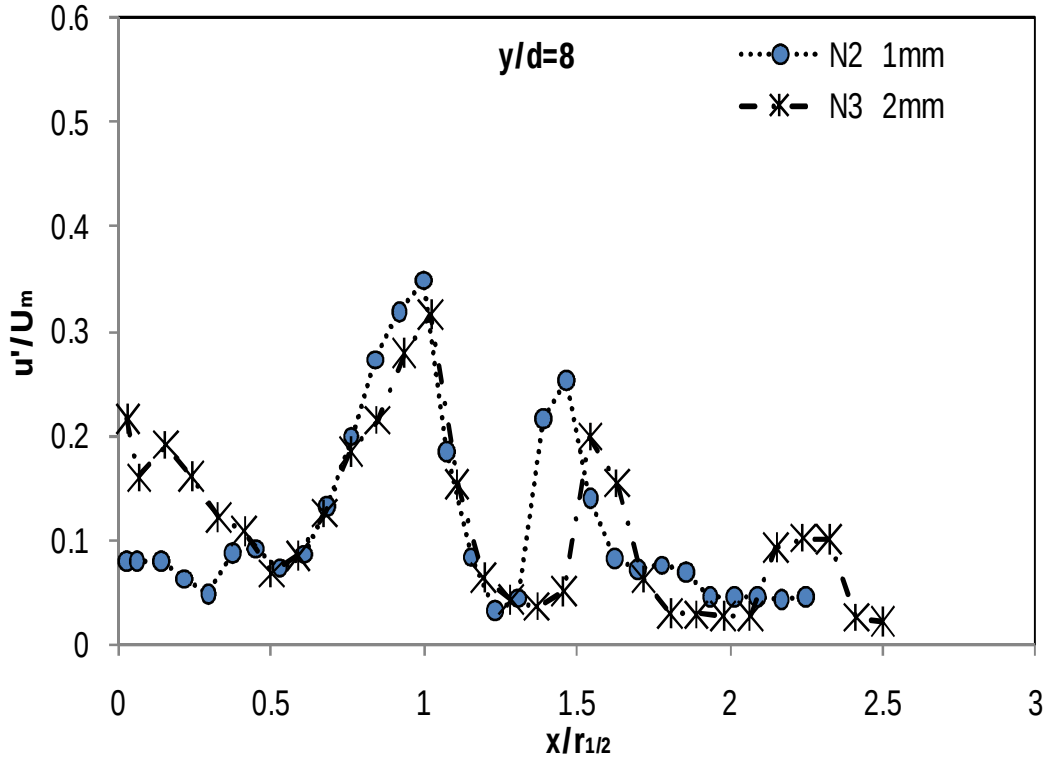

Figure C.4. Turbulent intensity profiles for the liquid jet at 0.170 *MPa* through the 1 and 2 *mm* diameter nozzles.

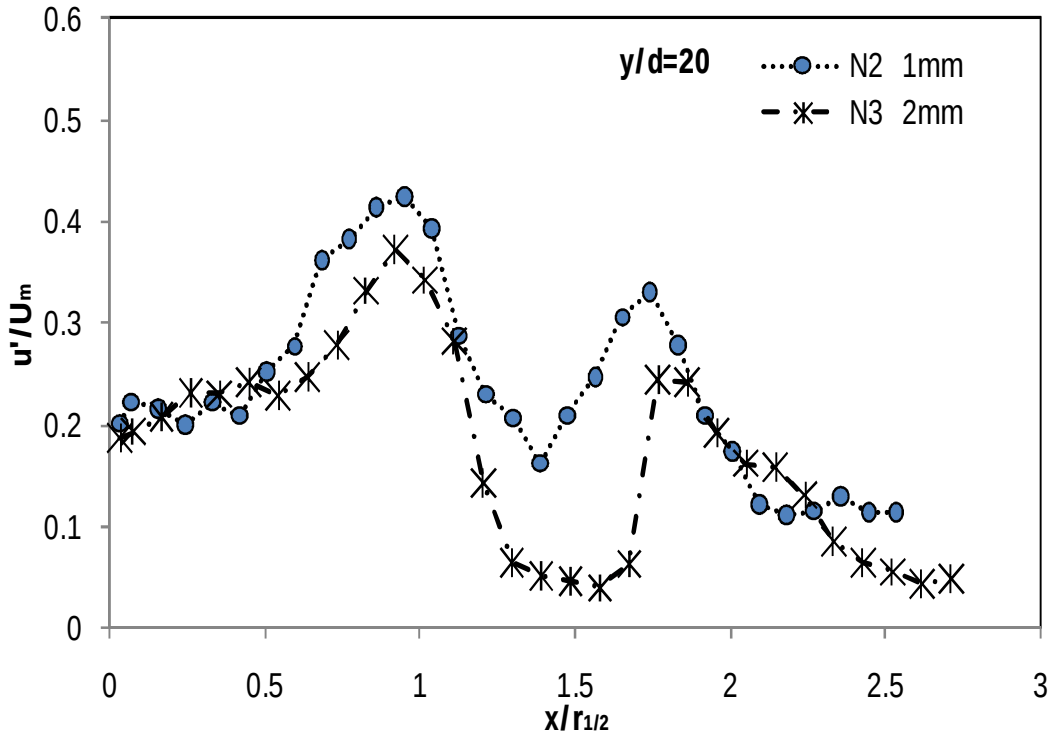

Figure C.5. Turbulent intensity profiles for the liquid jet at 0.377 *MPa* through the 1 and 2 *mm* diameter nozzles.

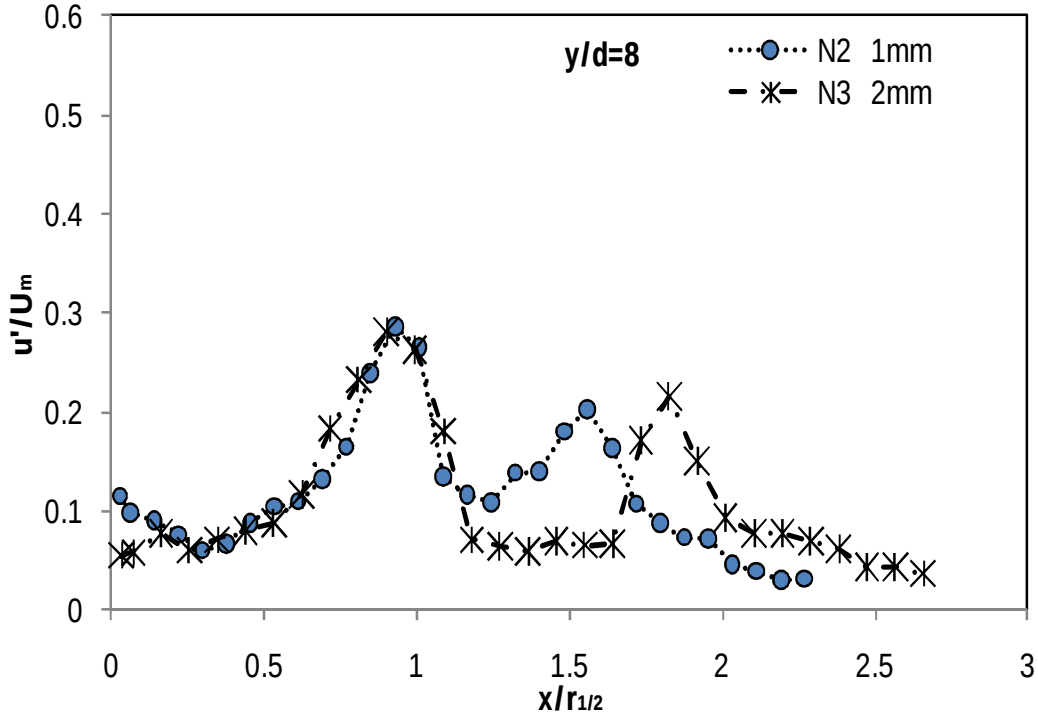

Figure C.6. Turbulent intensity profiles for the liquid jet at 0.584 *MPa* through the 1 and 2 *mm* diameter nozzles.

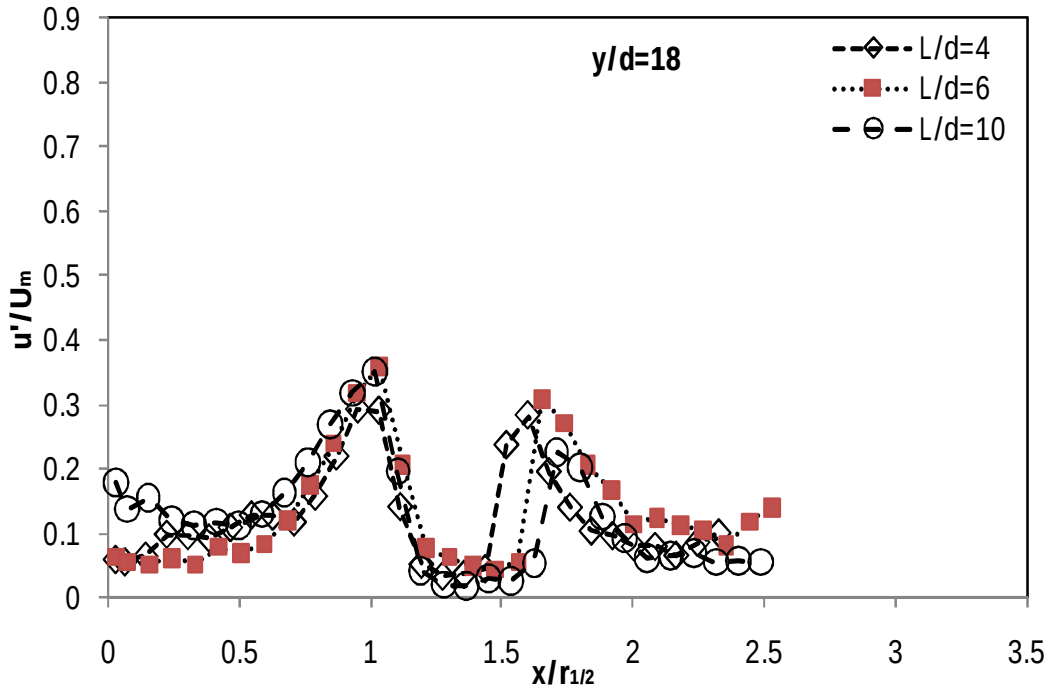

Figure C.7. Turbulent intensity profiles for the liquid jet at 0.170 *MPa* through nozzles with L/d of 4, 6 and 10.

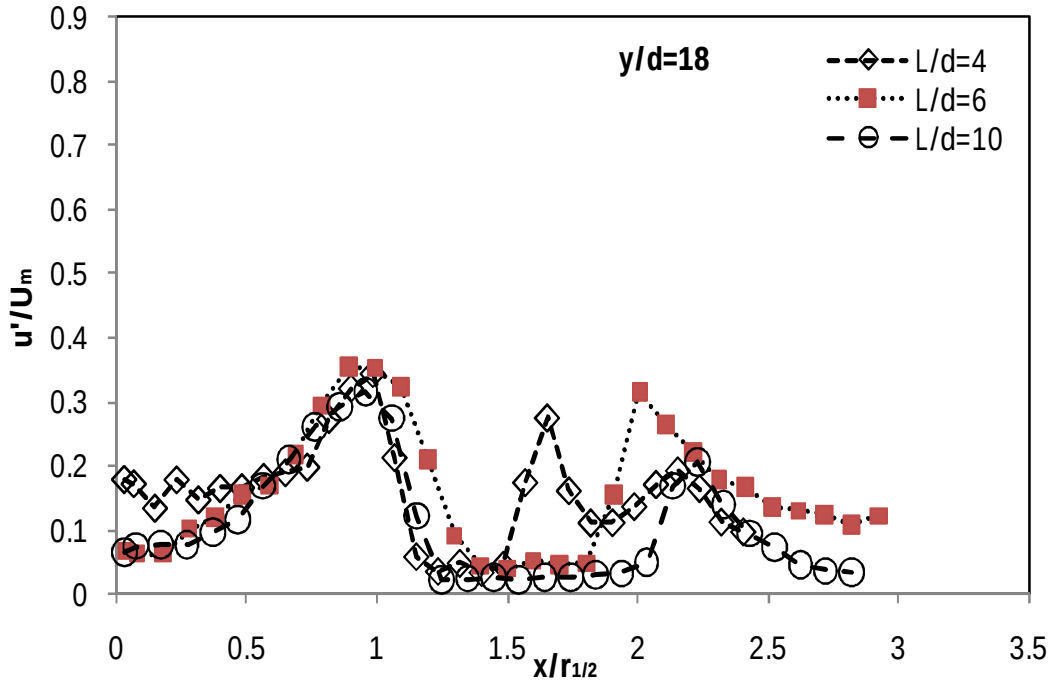

Figure C.8. Turbulent intensity profiles for the liquid jet at 0.377 *MPa* through nozzles with L/d of 4, 6 and 10.

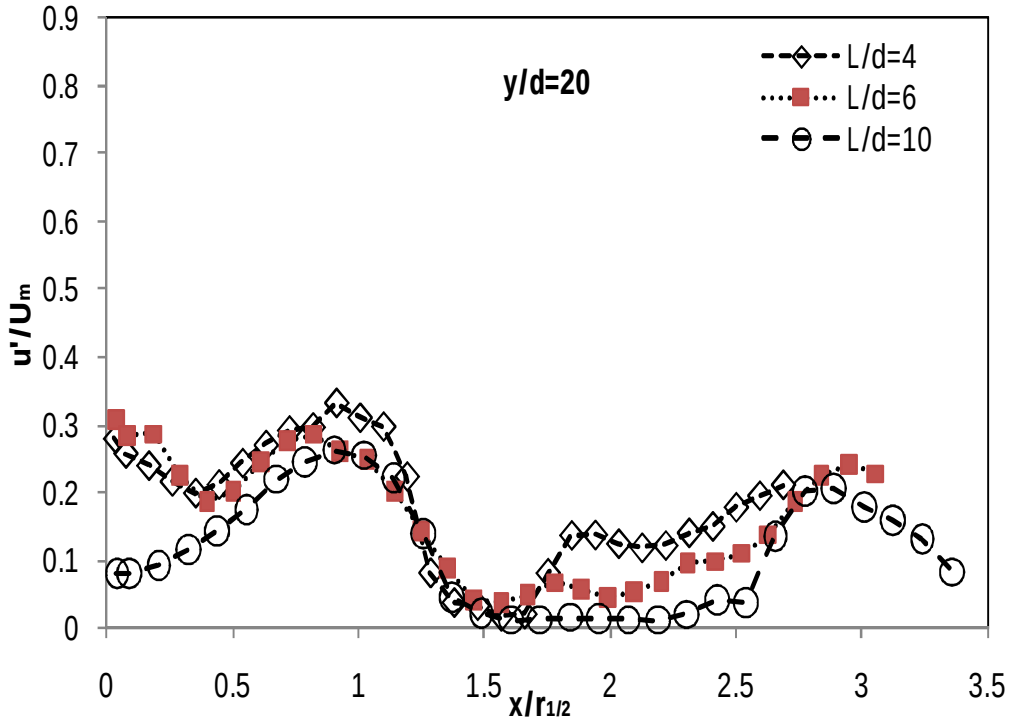

Figure C.9. Turbulent intensity profiles for the liquid jet at 0.584 *MPa* through nozzles with L/d of 4, 6 and 10**.**